10-25-2010

Geochemical Modeling of CO2 Sequestration in Dolomitic Limestone Aquifers

Mark W. Thomas
University of South Florida

Geochemical Modeling of CO_2 Sequestration in Dolomitic Limestone Aquifers

by

Mark W. Thomas

A thesis submitted in partial fulfillment
of the requirements for the degree of
Master of Science in Environmental Engineering
Department of Civil and Environmental Engineering
College of Engineering
University of South Florida

Major Professor: Jeffrey Cunningham, Ph.D.
Mark Stewart, Ph.D.
Maya Trotz, Ph.D.

Date of Approval:
October 25, 2010

Keywords: carbon capture and storage, activity coefficient, CO_2 solubility model, mineral precipitation and dissolution, geochemistry, non-linear

Acknowledgements

The research leading to this thesis was funded by the State of Florida through the Florida Energy Systems Consortium (FESC). Any opinions, findings, conclusions, or recommendations are those of the author and do not necessarily reflect the views of FESC.

I would like to thank Dr. Jeffrey Cunningham at the University of South Florida for giving me the opportunity to join his research team and become part of this project, and for the constructive comments, mentoring, and advice given during the writing of this thesis. I would also like to thank the faculty of the Department of Civil and Environmental Engineering at the University of South Florida for their teaching efforts, and to all those who encouraged me during the preparation of this thesis.

Table of Contents

List of Tables iii

List of Figures iv

Abstract vi

1: Introduction 1

2: Literature Review 5

3: Estimating Thermodynamic Variables 9

3.1: Equilibrium Constant, K 9

3.2: Activity Coefficient, γ 10

3.2.1: Activity Coefficient for Neutral Aqueous Species 11

3.2.2: Activity Coefficient for Charged Aqueous Species 11

3.2.3: Activity Coefficient for Aqueous CO_2 17

3.2.3.1: Method of Drummond (22) 18

3.2.3.2: Method of Rumpf et al. (23) 18

3.2.3.3: Method of Duan and Sun (25) 19

3.3: Estimating the Fugacity Coefficient for Gaseous and Supercritical CO_2, φ_{CO2} 20

3.3.1: Method of Spycher and Reed (26) 20

3.3.2: Method of Duan et al. (20) 21

3.4: Estimating the Activity of Water, a_W 21

3.5: Aqueous CO_2 Concentration, m_{CO2} 23

3.5.1: Equilibrium Constant 23

3.5.2: Method of Duan and Sun (25) 24

3.5.3: Method of Spycher and Pruess (21) 25

3.5.4: Spycher and Pruess (21) adaptation of the method of Duan and Sun (25) 27

3.6: Summary 29

4: Model Development 30

4.1: Model Overview 30
4.2: System of Geochemical Equations 30
4.2.1: Rock Minerals 31
4.2.2: Carbonate System 32
4.2.3: Aqueous Complexes 33
4.2.4: Salinity 34
4.2.5: Water (H_2O) System 35
4.2.6: Charge Balance 36
4.3: Iterative Solution Procedure 36
4.3.1: Inner Iteration Loop 37
4.3.2: Outer Iteration Loop 40
4.4: Model Implementation 41
4.5: Model Limitations 42
4.6: Model Outputs 42
4.7: Comparison of Thermodynamic Sub-models 43
5: Model Results 50
5.1: Effect of Initial pH 50
5.2: Effect of CO_2 Injection Pressure 54
5.3: Effect of Salinity 58
5.4: Effect of Temperature 62
5.5: Effects on Porosity, ε 65
5.6: Choice of Thermodynamic Sub-model for CO_2 Parameter Estimation 69
6: Summary and Conclusion 70
Works Cited 71

List of Tables

Table 1: Equilibrium Reactions for Mineral Dissolution and Precipitation 31

Table 2: Equilibrium Reactions for Carbonate Species 32

Table 3: Equilibrium Reactions for Aqueous Complexes.....33

Table 4: Equilibrium Reactions for H_2O Dissociation.....35

Table 5: Combinations of Sub-Models for CO_2 Thermodynamic Parameter Estimation 44

Table 6: Brine Densities at Various Salinities and Temperatures.....66

Table 7: Mineral Densities 67

Table 8: Porosity and Residual Brine Saturation Scenarios.....67

Table 9: Change in Porosity for Scenarios 1-3 Using Various Combinations of Initial pH, CO_2 Injection Pressure, Salinity, Temperature.....68

List of Figures

Figure 1: Debye-Huckel Parameter A_γ as a Function of Temperature at Constant Pressures 13

Figure 2: Debye-Huckel Parameter B_γ as a Function of Temperature at Constant Pressures 13

Figure 3: Helgeson Interaction Parameter b_{NaCl} as a Function of Temperature at Constant Pressures 16

Figure 4: Helgeson Interaction Parameter $b_{Na+,Cl-}$ as a Function of Temperature at Constant Pressures 17

Figure 5: Inner Iteration Loop for Pre-CO_2 Injection 37

Figure 6: Inner Iteration Loop for Post-CO_2 Injection 38

Figure 7: Outer Iteration Loop 41

Figure 8: Equilibrium pH for Various Choices of Thermodynamic Sub-Models 45

Figure 9: CO_2 Molality for Various Choices of Thermodynamic Sub-Models 45

Figure 10: Calcite Dissolution for Various Choices of Thermodynamic Sub-Models 46

Figure 11: Dolomite Dissolution for Various Choices of Thermodynamic Sub-Models 46

Figure 12: Gypsum Precipitation for Various Choices of Thermodynamic Sub-Models 47

Figure 13: Net CO_2 Storage for Various Choices of Thermodynamic Sub-models 47

Figure 14: Equilibrium pH as a Function of Initial pH 51

Figure 15: Calcite Dissolution as a Function of Initial pH 51

Figure 16: Dolomite Dissolution as a Function of Initial pH 52

Figure 17: Gypsum Precipitation as a Function of Initial pH 52

Figure 18: Net CO_2 Storage as a Function of Initial pH.....53

Figure 19: Equilibrium pH as a Function of CO_2 Injection Pressure.....54

Figure 20: Calcite Dissolution as a Function of CO_2 Injection Pressure 55

Figure 21: Dolomite Dissolution as a Function of CO_2 Injection Pressure.....55

Figure 22: Gypsum Precipitation as a Function of CO_2 Injection Pressure 56

Figure 23: Net CO_2 Storage as a Function of CO_2 Injection Pressure 56

Figure 24: Equilibrium pH as a Function of Salinity 58

Figure 25: Calcite Dissolution as a Function of Salinity.....59

Figure 26: Dolomite Dissolution as a Function of Salinity.....59

Figure 27: Gypsum Precipitation as a Function of Salinity 60

Figure 28: Net CO_2 Storage as a Function of Salinity.....60

Figure 29: Equilibrium pH as a Function of Temperature 62

Figure 30: Calcite Dissolution as a Function of Temperature.....63

Figure 31: Dolomite Dissolution as a Function of Temperature 63

Figure 32: Gypsum Precipitation as a Function of Temperature.....64

Figure 33: Net CO_2 Storage as a Function of Temperature.....64

Abstract

Geologic sequestration of carbon dioxide (CO_2) in a deep, saline aquifer is being proposed for a power-generating facility in Florida as a method to mitigate contribution to global climate change from greenhouse gas (GHG) emissions. The proposed repository is a brine-saturated, dolomitic-limestone aquifer with anhydrite inclusions contained within the Cedar Keys/Lawson formations of Central Florida. Thermodynamic modeling is used to investigate the geochemical equilibrium reactions for the minerals calcite, dolomite, and gypsum with 28 aqueous species for the purpose of determining the sensitivity of mineral precipitation and dissolution to the temperature and pressure of the aquifer and the salinity and initial pH of the brine. The use of different theories for estimating CO_2 fugacity, solubility in brine, and chemical activity is demonstrated to have insignificant effects on the predicted results. Nine different combinations of thermodynamic models predict that the geochemical response to CO_2 injection is calcite and dolomite dissolution and gypsum precipitation, with good agreement among the quantities estimated. In all cases, CO_2 storage through solubility trapping is demonstrated to be a likely process, while storage through mineral trapping is predicted to not occur. Over the range of values examined, it is found that net mineral dissolution and precipitation is relatively sensitive to temperature and salinity, insensitive to CO_2 injection pressure and initial pH, and significant changes to porosity will not occur.

1: Introduction

It is becoming increasingly accepted by the scientific community that global climate change due to anthropogenic emissions of greenhouse gases (GHG) is occurring. Greenhouse gases are being released at higher rate than the biosphere's ability to absorb them, with a resulting net increase of GHG concentrations in the atmosphere (1). A greenhouse gas of primary concern is carbon dioxide (CO_2). One of the major sources of CO_2 emissions is the combustion of fossil fuels for power generation and industrial processes in today's energy-intensive global economy (1). Part of the long-term solution to global climate change is widespread adoption of low carbon fuels for power generation and industrial processes; however, in the near term, techniques to reduce CO_2 emissions are being investigated (1).

One of the more promising mitigation techniques being investigated is capturing CO_2 from large point-source emitters and storing it to prevent release to the atmosphere (1; 2). This process, commonly referred to as carbon capture and storage (CCS), relies on technologies that have already been implemented at smaller scales by the oil and gas industries for enhanced oil recovery (EOR) and CO_2 disposal from natural gas refining (1; 2). Proposed repositories for large-scale storage of captured CO_2 include depleted oil and natural gas fields, coal beds, the deep ocean, and deep saline aquifers (1; 2). Deep saline aquifers are ideal candidates for storing CO_2 because they are commonly

found throughout the world, often have large storage capacity and ideal geologic properties, are not used as drinking water sources, and are isolated from the biosphere (1; 3; 4).

Injection of CO_2 into deep aquifers for geologic storage requires a compressed CO_2 stream recovered from industrial processes and an injection well drilled into the receiving formation (2). Typically, the CO_2 is injected into and maintained within the aquifer under supercritical conditions to take advantage of higher density of the CO_2 phase under these conditions; in other words, more mass of CO_2 is stored per bulk aquifer volume when it is supercritical versus when it is gaseous (1). As CO_2 injection into the aquifer continues, it will displace the native brine as it sweeps through the formation (2). As the native brine is being displaced by CO_2 sweeping, some brine will remain trapped in pores due to capillary forces. This trapped brine is known as the residual brine saturation, and may absorb CO_2 from the injected CO_2 phase.

Carbon dioxide storage in deep saline aquifers involves many uncertainties from geochemical and geologic perspectives. Carbon dioxide storage in a deep saline aquifer results in numerous geochemical reactions between the native brine and the rock minerals that comprise the aquifer formation (2; 4). These reactions are expected to result in dissolution and precipitation of different minerals, and this can have consequences related to formation integrity and storage efficiency (4). Excess mineral dissolution could weaken the aquifer formation, which could increase the risk of CO_2 escaping into other geologic formations (1; 5). Conversely, excess mineral precipitation could decrease the porosity of the formation, potentially decreasing the permeability of the aquifer to injected CO_2 or decreasing the available volume for bulk CO_2 storage (6).

The University of South Florida has been investigating the feasibility of capturing CO_2 from a power generating facility in Polk County, Florida and storing it in a deep, dolomitic-limestone aquifer located within the Cedar Keys/Lawson formation of Central Florida (7; 8; 9). Geochemical modeling of CCS in this formation has been previously performed by researchers at the University of South Florida using TOUGHREACT software (7). The previous models predicted that CO_2 injection in this formation would lower the pH of the native brine, resulting in the dissolution of calcite and dolomite and the precipitation of gypsum (7). Additionally, it was found that porosity increased very slightly due to excess mineral dissolution in areas where CO_2-saturated brine interacts with the mineral phase (7). However, further investigation into the methods used by the TOUGHREACT software for estimating thermodynamic parameters (activity coefficients, fugacity coefficients, solubility) is deemed warranted. Alternative geochemical models of CCS in the Cedar Keys/Lawson injection zone that yield similar predictions to those of TOUGHREACT simulations would lend support to the results reported by Cunningham et al. (7).

The first objective of this thesis is to develop a general thermodynamic framework for geochemical modeling of CO_2 injection into a dolomitic limestone aquifer that is representative of the Cedar Keys/Lawson injection zone. After developing a framework for geochemical modeling, the next objective is to examine the system sensitivity to different methods for estimating thermodynamic parameters for CO_2. The third objective is to investigate the system sensitivity to geophysical and chemical parameters like initial pH, CO_2 injection pressure, brine salinity, and temperature. The final objective of this

thesis is to use the results of the geochemical model to estimate changes in porosity induced by CO_2 injection.

This thesis will first discuss existing knowledge of CO_2 injection into deep saline aquifers (Chapter 2). It will then explore the thermodynamic variables involved in describing the geochemical system and different methods for their estimation (Chapter 3). This will be followed by discussion of the calculation methodology required to solve non-linear geochemical equations that describe the chemistry induced by CO_2 dissolution into residual brine (Chapter 4). Finally, data obtained from the models related to mineral precipitation and dissolution and changes in porosity will be presented (Chapter 5), and appropriate conclusions will be drawn (Chapter 6).

2: Literature Review

A great deal of research on CO_2 injection into geologic formations is available in the literature for a wide variety of conditions and intended purpose of storage. While the idea of widespread and large-scale capture and storage of CO_2 from facilities like fossil fuel power plants is relatively new, the process and technologies of injecting CO_2 underground are not (1; 10). Carbon dioxide injection has been used primarily in the oil industry as a way to increase oil production from declining fields and in the gas industry as a way to dispose of CO_2 that is stripped from natural gas during refining operations, though at a smaller scale than would be needed for widespread adoption of CO_2 sequestration from power generation facilities (1; 10). Much of the research has focused on CO_2 storage in sandstone formations because they often hold oil or natural gas and often include the possibility of mineral trapping due to the presence of aluminosilicate minerals (1; 11; 12). However, recent research has also considered the possibility of using carbonate formations as CO_2 storage repositories (5; 6; 13). Studies have included both laboratory experiments and computer modeling of expected conditions for a CO_2 injection process into a carbonate aquifer (4; 5; 6; 13; 14).

Carbon dioxide is trapped in a deep saline aquifer by several processes. Initially, CO_2 is trapped within the pores of the aquifer formation due to capillary forces and underneath the aquifer confining layer by hydrodynamic forces due to buoyancy (1; 2). As time passes, CO_2 is further trapped in the aquifer by dissolution and speciation into

native brine through solubility and ionic trapping (1; 2). Finally, dissolved carbonate species can be further trapped by combining with dissolved cations to form solid mineral precipitates in thermodynamic equilibrium with the brine during a process known as mineral trapping (1; 2).

It has been suggested that mineral trapping of CO_2 in a typical calcium carbonate aquifer (i.e. calcium or calcite is present in significant amounts) is not a viable mechanism for CO_2 storage due to the increase in solubility of calcium carbonate minerals at low pH conditions resulting from CO_2 dissolution into native brine (4; 6; 13). This is in contrast to the precipitation of low-solubility carbonate minerals that is expected in aluminosilicate-rich, iron-rich, or magnesium-rich aquifer formations (3; 10; 11). Modeling performed by others typically predicts a pH around 4.8 as a result of CO_2 dissolution into brine contained within a carbonate aquifer (5; 7). Solution buffering by bicarbonate ion (HCO_3^-) due to dissolution of carbonate-containing minerals is predicted to be the dominant mechanism for determining the pH of CO_2-saturated brine in carbonate aquifers (4; 5; 7). Additionally, solution buffering enhances the dissolution of CO_2, and this can contribute to additional CO_2 storage by solubility trapping (5; 15). Calcite, if present, is always predicted to dissolve locally when it is in contact with CO_2-saturated brine (5; 6; 7; 13), although some studies have found that it can precipitate downstream from areas of high dissolution due to particle trapping in pores and exposure to high bicarbonate concentration in displaced brine (6). The net calcite dissolution is predicted to be relatively low when compared to its abundance in the mineral phase (i.e., aquifer matrix) (5; 7). However, near the injection well, some have noted that calcite dissolution can be quite high, leading to large increases in porosity with high connectivity

– i.e. channeling through the rock formation (4). Dolomite, if it is also present in the mineral phase, has been predicted by some models to dissolve along with calcite when in contact with CO_2 saturated brine (5; 7). However, other models predict that dolomite can precipitate when magnesium-saturated brine encounters a pure calcite phase (13). Cunningham et al. also suggest that gypsum precipitates due to increased Ca^{2+} concentrations released by calcite and dolomite dissolution when sulfate ion (SO_4^{2-}) is present (7).

In the literature, most computer models of single-phase CO_2 injection into carbonate aquifers typically predict that that permeability and porosity are not likely to be significantly affected (5; 7; 13). However, some research suggests that micro-scale anisotropic features of the aquifer formation can influence mineral dissolution and precipitation and have a significant effect on changes in porosity and permeability (13; 14). This is consistent with lab experiments performed by Izgec et al. (6). Others have explored the difference between injecting pure-phase CO_2 versus CO_2-saturated brine and found that injection of CO_2-saturated brine can damage the aquifer formation by excessive carbonate mineral dissolution. This is a result of continuous refreshing of CO_2-saturated brine that is cation-deficient near the wellhead (4). In general, however, most studies do not predict that changes in porosity and permeability due to geochemical effects of CO_2 injection into carbonate aquifers represent a significant impediment to implementation (4; 5; 7).

Most research into the geochemical effects of CO_2 injection into a carbonate aquifer suggests that carbonate minerals will dissolve. However, there is some disagreement over the extent of carbonate mineral dissolution and the effects of this dissolution on porosity

and permeability. Furthermore, there is a lack of data comparing the effects of the choices of different methods for estimating thermodynamic parameters on the geochemical system. Finally, there is little information available in the literature on the sensitivity of the geochemistry involved with CO_2 injection into a carbonate aquifer to physical and chemical parameters like initial pH, CO_2 injection pressure, and brine salinity.

3: Estimating Thermodynamic Variables

To model the effects of CO_2 injection into a carbonate aquifer, the system must be described in a thermodynamic context. This thermodynamic description is based on solubility equilibrium relationships for minerals, aqueous complexes, and CO_2 with ions dissolved in the native brine of the aquifer formation. Deviations from ideal thermodynamic behavior due to high pressure, salinity, and temperature are accounted for by activity coefficients for aqueous species and by a fugacity coefficient for the supercritical CO_2 phase.

3.1: Equilibrium Constant, *K*

The equilibrium constant, *K*, represents the ratio of product activities to reactant activities that occurs when the forward and reverse rates of a reaction are equal (i.e., the reaction is at equilibrium). Consider a chemical reaction where the reactants *A* and *B* are in equilibrium with the products *C* and *D*. The reaction can be written in the following manner:

$$aA + bB \overset{eq}{\Leftrightarrow} cC + dD \qquad \text{Equation 1}$$

where lowercase letters represent a stoichiometric coefficient and uppercase letters represent a chemical species. The equilibrium constant is given by the following expression:

$$K = \frac{(a_C)^c (a_D)^d}{(a_A)^a (a_B)^b}$$ Equation 2

where a_j represents the chemical activity of species j.

Equilibrium constants for many reactions have been determined experimentally and values are available in the literature. For this study, equilibrium constants are taken from the thermodynamic database included with the TOUGHREACT geochemical modeling software (16). This database has equilibrium constants for many geochemical reactions as functions of temperature and is considered valid over a temperature range of 0-300°C (16). The equilibrium constants for most reactions considered in this paper are calculated using an equation of the following form (16):

$$\log K = a \ln T + b + cT + \frac{d}{T} + \frac{e}{T^2}$$ Equation 3

where K is the equilibrium constant, T is the temperature in Kelvin and a through e are constants that are defined in the geochemical database for each equilibrium reaction (16). Most of the geochemical reactions considered in this thesis are analyzed using equilibrium constants.

3.2: Activity Coefficient, γ

The activity coefficient, γ, relates the activity of a chemical species to its concentration, and is a way to account for non-ideal effects that occur at high ionic strength, temperature, and pressure. The following equation describes the relationship between chemical activity and the activity coefficient:

$$a_i = \gamma_i m_i$$ Equation 4

where a_i is the activity of chemical i and m_i represents the molal concentration of i. The activity coefficient must be estimated for the following three types of aqueous species: neutral, ionic, and dissolved CO_2. Methods for estimating activity coefficients for these different types of aqueous species are described below.

3.2.1: Activity Coefficient for Neutral Aqueous Species

A neutral species is a solvated complex containing positive and negative ions with a net charge of zero. Examples include $NaHCO_{3(aq)}$, $NaCl_{(aq)}$, $CaCO_{3(aq)}$, etc. The activity of aqueous neutral species is assumed to be equal to unity (11; 16).

3.2.2: Activity Coefficient for Charged Aqueous Species

Charged aqueous species includes ions and charged aqueous complexes. When charged species are dissolved in a solvent that contains high concentrations of other charged species, the effects of individual species are dampened due to ionic interactions. This dampening effect is quantified by the activity coefficient, γ. In general, charged aqueous species have activity coefficients that are less than unity.

To calculate the activity coefficient for charged aqueous species, the method presented by Helgeson et al. (17) is used. This method is chosen because it is applicable for temperatures between 0-600°C, pressures up to 5000 bar, and chloride brines up to 6 molal ionic strength (16; 17). This is the calculation method that is used in the TOUGHREACT software (16). The expression for estimating activity coefficients of charged aqueous species is as follows (16; 17):

$$\log\gamma_j = -\frac{A_\gamma (z_j)^2 \sqrt{\bar{I}}}{1 + \mathring{a}_j B_\gamma \sqrt{\bar{I}}} - \log\left(1 + \frac{m^*}{55.51}\right) + \left[\omega_{abs,j} b_{NaCl} + b_{Na^+,Cl^-} - 0.19(|z_j| - 1)\right]\bar{I} \quad \text{Equation 5}$$

where A_γ and B_γ are Debye-Huckel parameters; z_j is the ionic charge for charged species j; $\bar{I}$ is the true ionic strength in molal units; $\mathring{a}_j$ is the ion distance of closest approach for ion j; m^* is the sum of molal concentrations for all dissolved species; $\omega_{abs,j}$ is the absolute Born coefficient for charged species j; and b_{NaCl} and b_{Na^+,Cl^-} are parameters describing ionic interaction.

The equations to estimate Debye-Huckel parameters A_γ and B_γ were regressed as functions of temperature and pressure using data given in Tables 1 and 2 of Helgeson et al. (18). These tables contain experimental data values for these Debye-Huckel parameters at different temperatures for the saturation pressure of water and five constant pressures ranges between 1 kilobar and 5 kilobar. Linear interpolation is used for estimating values that lie between the constant pressure lines. Plots of A_γ and B_γ as functions of temperature for the different pressures are obtained using data from the literature (18) and are presented in the following figures:

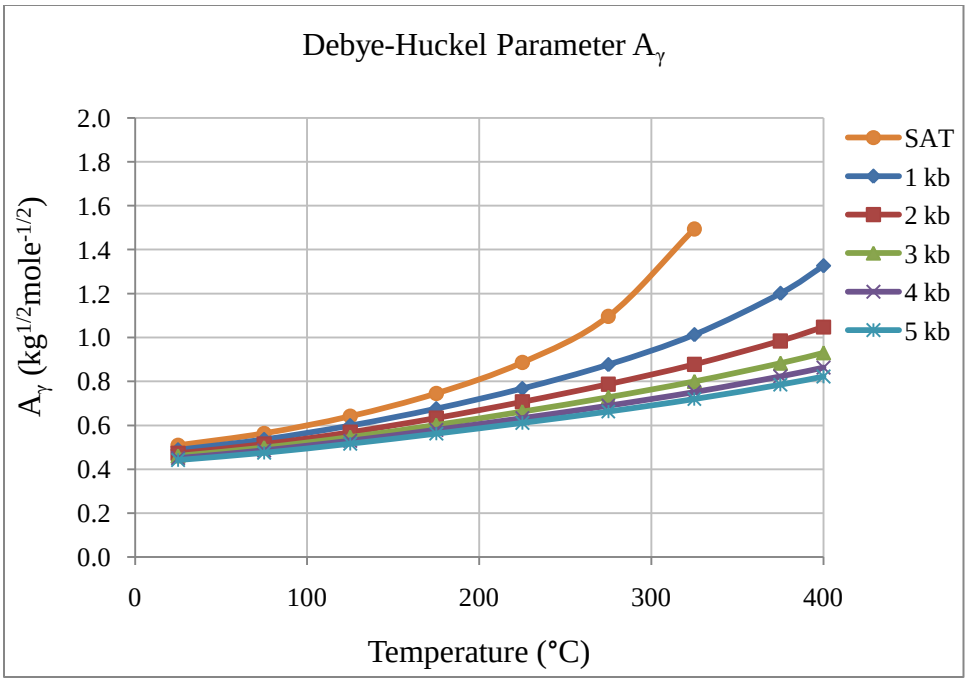

Figure 1: Debye-Huckel Parameter A_γ as a Function of Temperature at Constant Pressures

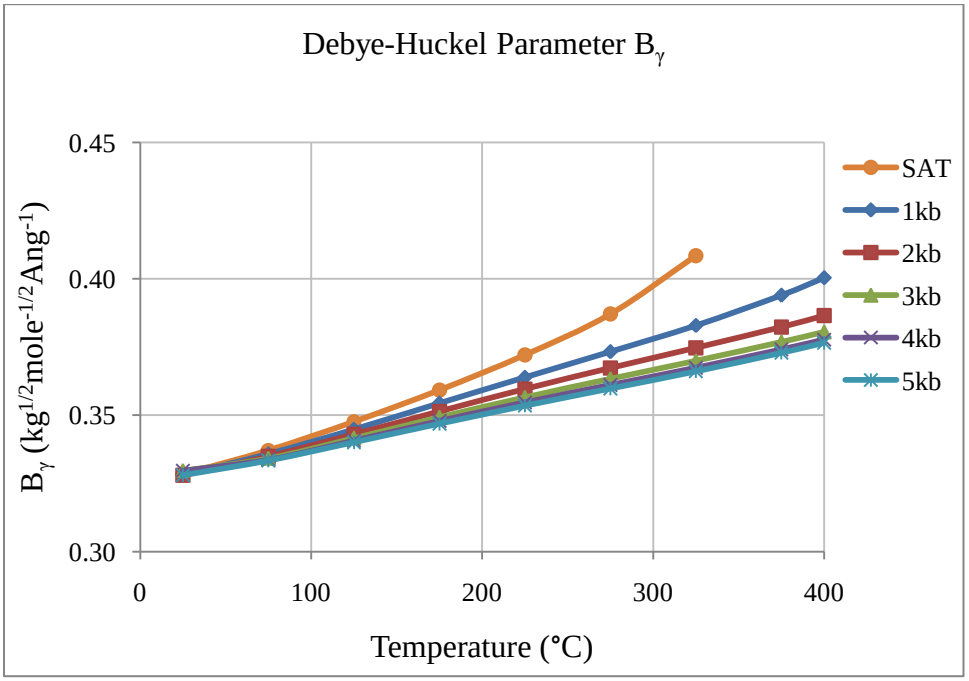

Figure 2: Debye-Huckel Parameter B_γ as a Function of Temperature at Constant Pressures

The true ionic strength is given by the following equation (17):

$$\bar{I} = \frac{1}{2}\left(\sum_j m_j z_j^2 + \sum_q m_q z_q^2\right) \qquad \text{Equation 6}$$

where m represents molal concentration, subscript j represents free ionic species and subscript q represents aqueous complexes. This is different from the stoichiometric ionic strength, where the concentrations in the calculation do not take into account whether the ions are complexed with other ions. Stoichiometric ionic strength is defined by the following equation (17):

$$I = \frac{1}{2}\left(\sum_j m_j z_j^2 + \sum_q \nu_j m_{q,j} z_j^2\right) \qquad \text{Equation 7}$$

where m_j represents the molal concentration of the free ion j, ν_j is the stoichiometric coefficient of species j combined in aqueous complex q, and $m_{q,j}$ represents the molal concentration of aqueous complex q containing ion j. Note that in the aqueous complex summation operator, the charge of ion j is used for calculations, as opposed to the charge of aqueous complex q used in the true ionic strength calculation.

The distance of closest approach, $\mathring{a}_j$, for charged species interactions is based on the assumption that most ionic interactions will involve Na^+ and Cl^- ions due to their high concentrations (16; 19). This implies that most charged species are shielded by surrounding Na^+ or Cl^- ions, depending on the respective charges. The distance of closest approach is calculated as follows (16; 17; 19):

$$\mathring{a}_j = 2\left(\frac{r_{eff,j} + 1.91|z_j|}{|z_j| + 1}\right) \text{ for anions} \qquad \text{Equation 8}$$

$$\mathring{a}_j = 2\left(\frac{r_{eff,j} + 1.81|z_j|}{|z_j| + 1}\right) \text{ for cations} \qquad \text{Equation 9}$$

where $r_{eff,j}$ is the effective ionic radius of species j in Angstroms. These expressions are based on simplifications of Equation 125 of Helgeson et al. (17) by Reed (19) as explained in the TOUGHREACT user guide (16). Values for r_{eff} are taken from Table 3 of Helgeson et al. (17). Note that 1.91 and 1.81 are the ionic radii in Angstroms for Na^+ and Cl^-, respectively.

The absolute Born coefficient for ion j, $\omega_{abs,j}$, is an ion solvation parameter and is calculated as follows (16; 17):

$$\omega_{abs,j} = \frac{\eta(z_j)^2}{r_{eff,j}} \qquad \text{Equation 10}$$

where η = 1.66027·10^5 Ang-cal/mole and $r_{eff,j}$ is in Angstroms. It is related to the dielectric constant of the solution (17).

Calculating the interaction parameters b_{NaCl} and b_{Na^+,Cl^-} follows a procedure similar to that used for calculating the Debye-Huckel parameters. Equations were regressed based on data given in Tables 29 and 30 of Helgeson et al. (17) as functions of temperature for the saturation vapor pressure for water and at five additional constant pressures ranging from 1 kilobar to 5 kilobar. Linear interpolation is used to estimate values for interaction

parameters that lie between constant pressure lines. Plots of b_{NaCl} and b_{Na^+,Cl^-} are given in the following figures:

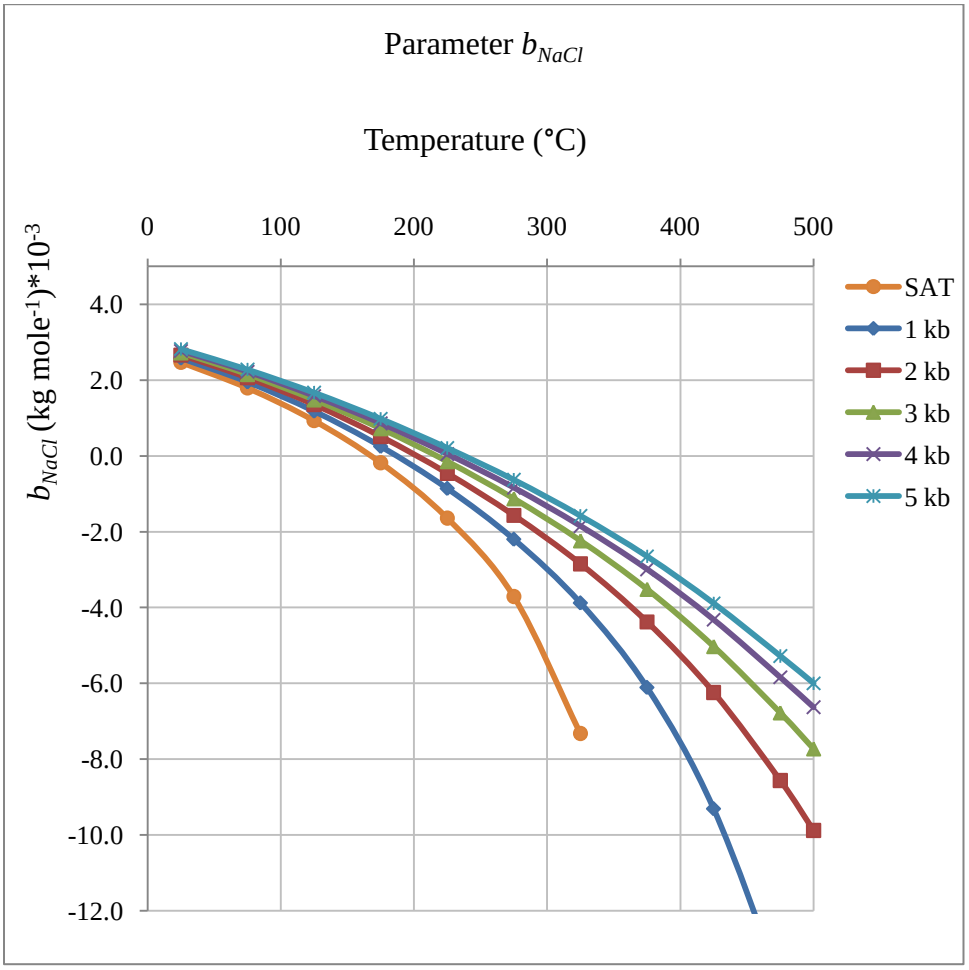

Figure 3: Helgeson Interaction Parameter b_{NaCl} as a Function of Temperature at Constant Pressures

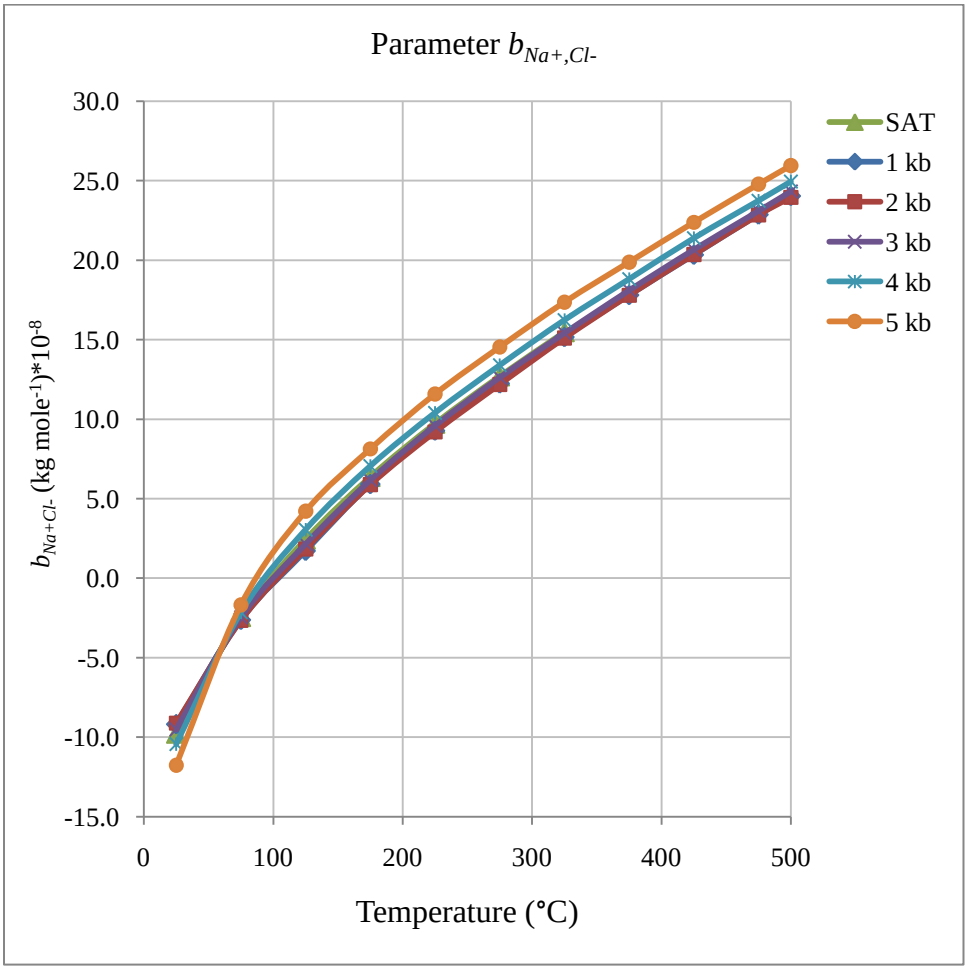

Figure 4: Helgeson Interaction Parameter $b_{Na+,Cl-}$ as a Function of Temperature at Constant Pressures

In summary, Equations 5, 6, and 8-10 are used with data given in Figures 1-4 to estimate the activity coefficient for each species of dissolved ion and charged aqueous complex.

3.2.3: Activity Coefficient for Aqueous CO_2

The activity coefficient for aqueous (dissolved) CO_2 describes the non-ideal effects of high temperature, pressure, and ionic strength on the chemical activity of $CO_{2(aq)}$. This

coefficient is used to account for the "salting-out" effect that decreases CO_2 solubility in high ionic strength solutions as compared with pure water (16; 20). At low ionic strengths, the activity coefficient for dissolved CO_2 is considered to be unity (16; 21). However, the activity coefficient increases at high ionic strength as the solution becomes more "crowded" for dissolved CO_2 and dissolution is less than predicted based on ideal thermodynamic considerations. For this study, three different models are used to estimate γ_{CO2}.

3.2.3.1: Method of Drummond (22)

This model is a function of temperature and ionic strength and is given by the following expression (16; 22):

$$\ln \gamma_{CO2} = \left(C + FT + \frac{G}{T}\right) I - (E + HT)\left(\frac{I}{I+1}\right) \qquad \text{Equation 11}$$

where *T* is the temperature in Kelvin; *I* is the molal ionic strength; and *C, F, G, E* and *H* are constants tabulated by Drummond (16; 22). This model has been cited in numerous publications and has been incorporated into TOUGHREACT geochemical modeling software as well as others (16). This model is valid for a temperature range of 20-400 °C and 0-6.5 molal NaCl concentration and yields the molal scale activity coefficient for aqueous CO_2 (16; 22).

3.2.3.2: Method of Rumpf et al. (23)

This model is a function of temperature and ionic strength and is given by the following expression (21; 23):

$$\ln \gamma_{CO2} = 2m_{salt}B^{(0)} + 3(m_{salt})^2\Gamma \qquad \text{Equation 12}$$

where (21; 23):

$$B^{(0)} = 0.254 - \frac{76.82}{T} - \frac{10656}{T^2} + \frac{6312 \times 10^3}{T^3} \quad \text{Equation 13}$$

and (21; 23):

$$\Gamma = -0.0028 \quad \text{Equation 14}$$

where T is the temperature in Kelvin and m_{salt} is the molal concentration of all dissolved salt species. A variation presented by Spycher et al. (21) based on a simplification presented by Duan et al. (24) is included to yield the final form of the equation (21):

$$\ln \gamma_{CO2} = 2B^{(0)}\left(m_{Na} + m_K + 2m_{Ca} + 2m_{Mg}\right) + 3\Gamma m_{Cl}\left(m_{Na} + m_K + m_{Ca} + m_{Mg}\right) \quad \text{Equation 15}$$

where m is the molal concentration of the indicated species. This method is valid for temperature from 313-433 K and 0-6 molal salt concentration and yields a molal scale activity coefficient (21).

3.2.3.3: Method of Duan and Sun (25)

This model is a function of temperature, pressure, and ionic strength, and is given by the following expression (25):

$$\ln \gamma_{CO2} = 2\lambda\left(m_{Na} + m_K + 2m_{Ca} + 2m_{Mg}\right) + \zeta m_{Cl}\left(m_{Na} + m_K + m_{Ca} + m_{Mg}\right) - 0.07 m_{SO4} \quad \text{Equation 16}$$

where λ and ζ are parameters calculated based on the following equation (25):

$$Par(T,P) = c_1 + c_2T + \frac{c_3}{T} + c_4T^2 + \frac{c_5}{(630-T)} + c_6P + c_7P\ln T + \frac{c_8P}{T} + \frac{c_9P}{(630-T)} + \frac{c_{10}P^2}{(630-T)^2} + c_{11}T\ln P \quad \text{Equation 17}$$

where P is the pressure in bars, T is the temperature in Kelvin, and c_1 through c_{11} are constants from Table 2 of Duan and Sun (25). Note that λ and ζ use different sets of constants c_1 through c_{11}. This CO_2 activity coefficient model is valid for temperatures of 273-573 K, pressures of 0-2000 bar and ionic strengths of 0-4.3 molal (25).

3.3: Estimating the Fugacity Coefficient for Gaseous and Supercritical CO_2, φ_{CO2}

The fugacity coefficient, φ_{CO2}, is a parameter used to describe the deviation from ideal thermodynamic behavior of gaseous/supercritical CO_2 that is observed at high temperature and pressure. The fugacity coefficient is used to calculate the fugacity of the $CO_{2(g,sc)}$ phase, a thermodynamic value that is akin to the activity of an aqueous species. Gas phase fugacity is calculated as follows:

$$F = \varphi_{CO2} * P_{CO2} \quad \text{Equation 18}$$

where F is the fugacity, φ is the fugacity coefficient, and P_{CO2} is the partial pressure of CO_2 in bars. For this study, two models are used to estimate φ_{CO2} as described below.

3.3.1: Method of Spycher and Reed (26)

This model, a function of temperature and pressure, is given by the following expression (26):

$$\ln \varphi_{CO2} = \left(\frac{a}{T^2} + \frac{b}{T} + c\right)P + \left(\frac{d}{T^2} + \frac{e}{T} + f\right)\frac{P^2}{2} \quad \text{Equation 19}$$

where *T* is the temperature in Kelvin; *P* is the total gas pressure in bars; and *a, b, c, d, e* and *f* are constants given by Spycher and Reed (26). This model is applicable for a temperature range of 50-350°C and pressure up to 500 bars (26). It is reported that there are significant discrepancies between the estimated compressibility factor, *Z*, using this model and experimentally observed values of *Z* at the *P-T* ranges considered (26). This indicates that the method of Spycher and Reed (26) might not be the best method for estimating the CO_2 fugacity coefficient. However, this model has been incorporated into the geochemical modeling software TOUGHREACT (16) and is thus considered in this thesis.

3.3.2: Method of Duan et al. (20)

This model, also a function of temperature and pressure, is given by the following expression (20):

$$\varphi_{CO2} = c_1 + \left[c_2 + c_3 T + \frac{c_4}{T} + \frac{c_5}{(T-150)}\right] P + \left[c_6 + c_7 T + \frac{c_8}{T}\right] P^2 + \left[c_9 + c_{10} T + \frac{c_{11}}{T}\right] \ln P + \frac{[c_{12} + c_{13} T]}{P} + \frac{c_{14}}{T} + c_{15} T^2 \quad \text{Equation 20}$$

where *T* is the temperature in Kelvin, *P* is the pressure in bars, and $c_1 - c_{15}$ are constants given in Table 1 of Duan et al. (20). This model has been fitted to experimental data for six T-P ranges ranging from 273-573K and 0-2000 bar (20).

3.4: Estimating the Activity of Water, a_W

The activity of water, a_W, is considered to be unity under ideal conditions. However, at elevated temperature, pressure, and ionic strength, the activity of water begins to deviate from unity as a function of the osmotic coefficient, Φ (16; 17):

$$\ln a_W = -\Phi \frac{m^*}{55.51} \quad \text{Equation 21}$$

where m^* is the total molal concentration of all dissolved ions. The osmotic coefficient, Φ, is calculated as follows (16):

$$\Phi = \frac{-2.303}{m^*} \sum_j \left[m_{t,j} \left[\frac{A_\gamma z_j^2 I^{0.5} \sigma}{3} + \frac{\log\left(1 + {m^*}/{55.51}\right)}{{m^*}/{55.51}} - 0.50 \left(I \omega_{abs,j} b_{NaCl} + \left[b_{Na^+,Cl^-} - 0.19\left(|z_j| - 1\right) \right] \frac{m_{CHRG}}{2} \right) \right] \right] \quad \text{Equation 22}$$

where (16; 17):

$$\sigma = \frac{3}{\text{å}^3 B_\gamma^3 I^{1.5}} \left(\Lambda - \frac{1}{\Lambda} - 2 \ln \Lambda \right) \quad \text{Equation 23}$$

where (16; 17):

$$\Lambda = 1 + \text{å} B_\gamma \sqrt{I} \quad \text{Equation 24}$$

where I is the stoichiometric ionic strength (see Equation 7), $m_{t,j}$ is the total molal concentration of ion j, and m_{CHRG} is the total molal concentration of all charged species in solution. This procedure for calculating the osmotic coefficient utilizes several modifications presented in the TOUGHREACT user manual (16). The original form of the osmotic coefficient equation is Equation 190 of Helgeson et al. (17); and assuming NaCl dominance in solution, would yield this expression (17):

$$\Phi = \frac{-2.303}{m^*}\sum_j \left[m_{t,j} \left[\frac{A_\gamma z_j^2 I^{0.5}\sigma}{3} + \frac{\log\left(1 + {m^*}/{55.51}\right)}{{m^*}/{55.51}} - 0.50\bar{I}\left(\omega_{abs,j} b_{NaCl} + b_{Na^+,Cl^-} - 0.19\left[\left|z_j\right| - 1\right]\right) \right] \right] \quad \text{Equation 25}$$

Note that this is a function of the true ionic strength, $\bar{I}$ (see Equation 6). However, it is reported in the TOUGHREACT user guide (16), and implemented in the TOUGHREACT program, that using the stoichiometric ionic strength and half the charged species molality more accurately matches experimentally obtained data than the original formulation based solely on the true ionic strength (16).

3.5: Aqueous CO_2 Concentration, m_{CO2}

The molal concentration of dissolved CO_2 in brine is estimated using four methods.

3.5.1: Equilibrium Constant

This method is based on the equilibrium expression for the following chemical reaction:

$$\mathrm{CO_{2(g,sc)}} + \mathrm{H_2O} \overset{\text{eq}}{\Leftrightarrow} \mathrm{H^+} + \mathrm{HCO_3^-} \quad \text{Equation 26}$$

$$K_{CO2(g,sc)} = \frac{a_{H^+} a_{HCO_3^-}}{F_{CO2} a_W} \quad \text{Equation 27}$$

where F_{CO2} is the fugacity of gaseous/supercritical CO_2, which is estimated using techniques discussed in Section 3.3. The activity of bicarbonate ion is constrained additionally by equilibrium with dissolved CO_2 according to the following equations:

$$CO_{2(aq)} + H_2O \overset{eq}{\Leftrightarrow} H^+ + HCO_3^- \quad \text{Equation 28}$$

$$K_{CO2(aq)} = \frac{(a_{H^+})(a_{HCO_3^-})}{(a_{CO_{2(aq)}})(a_W)} \quad \text{Equation 29}$$

The value for $K_{CO2(aq)}$ is taken from thermodynamic database included with TOUGHREACT geochemical modeling software and is calculated as a function of temperature. At 45°C, the log $K_{CO2(aq)}$ value is -6.273 (16). The activity of $CO_{2(aq)}$ is related to the molal concentration of CO_2 by the following equation:

$$m_{CO2} = \frac{a_{CO_{2(aq)}}}{\gamma_{CO2}} \quad \text{Equation 30}$$

The equations simplify to yield an expression for m_{CO2} as a function of CO_2 fugacity, equilibrium constants, and activity coefficient. The concentration of dissolved CO_2, along with the solution pH, is used to estimate the activity of bicarbonate, HCO_3^-, which all other geochemical species are functions of. The pH is then iterated until the geochemical system converges.

3.5.2: Method of Duan and Sun (25)

This model is a function of temperature, pressure and salt content, and is given by Equation 9 of Duan and Sun (25):

$$\ln m_{CO2} = \ln(y_{CO2}P_{TOT}\varphi_{CO2}) - {\mu_{CO2}^{1(0)}}/{RT} - 2\lambda(m_{Na} + m_K + 2m_{Ca} + 2m_{Mg}) - \zeta m_{Cl}(m_{Na} + m_K + m_{Ca} + m_{Mg}) + 0.07m_{SO4} \quad \text{Equation 31}$$

where y_{CO2} is the CO_2 mole fraction in the gaseous phase (assumed in this study to be unity) and $\mu_{CO2}^{1(0)}$ is the difference between the chemical potentials of CO_2 in the gaseous phase and the liquid phase (20). The value of $\mu_{CO2}^{1(0)}/RT$ is calculated similarly to λ and ζ using constants given in Table 2 of Duan and Sun (2003). This CO_2 solubility model is valid for temperatures of 273-573K, pressures of 0-2000 bar and ionic strengths of 0-4.3 m, and yields values that are within 10% of experimentally observed values (20).

3.5.3: Method of Spycher and Pruess (21)

This model is a function of temperature, pressure and salt content, and is given by Equation 2 of Spycher and Pruess (21):

$$x_{CO2} = \frac{\Phi_{CO2}(1 - y_{H2O})P_{TOT}}{55.51\gamma_x' K^0_{CO2(g)}} exp\left(\frac{-[P - P^0]\bar{V}}{RT}\right) \qquad \text{Equation 32}$$

where y_{H2O} is the water mole fraction in the gaseous phase (assumed to be zero for this study); γ_x' is the mole fraction scale activity coefficient for aqueous CO_2; K_{CO2}^0 is the thermodynamic equilibrium constant for CO_2 dissolution; P^0 is 1 bar; and $\bar{V}$ is the average partial molar volume of CO_2 over the $P^0 \rightarrow P$ range, which is assumed to be 32.6 cm^3/mole based on data in Table 2 of Spycher and Pruess (21).

To calculate K_{CO2}^0, the following equation is used (21):

$$K^0_{CO2(g)} = a + bT + cT^2 + dT^3 \qquad \text{Equation 33}$$

where *a*, *b*, *c* and *d* are constants given in Table 2 of Spycher and Pruess (21) and *T* is temperature in degrees Celsius.

The mole fraction activity coefficient for CO_2 can be converted from the molal scale activity coefficient (see Section 3.2.3:) with the following equation (21):

$$\gamma_x' = \gamma_m' \left[\frac{(1 + m_{CO2} + m_{salt})/55.51}{1 + m_{CO2}/55.51} \right] \quad \text{Equation 34}$$

where m_{salt} is the total molal concentration of all species that are not aqueous CO_2 and γ_m' is the molal scale activity coefficient that is calculated using methods presented earlier. It is reported by Spycher and Pruess (21) that more accurate results are obtained using the methodology of Duan and Sun (25) or Rumpf et al. (23) for calculating γ_m'.

The molal concentration of aqueous CO_2 can be determined from the mole fraction of aqueous CO_2 using the following relationship (21):

$$m_{CO2} = \frac{x_{CO2}(m_{salt} + 55.51)}{1 - x_{CO2}} \quad \text{Equation 35}$$

Unlike the previous two models for CO_2 aqueous solubility, this model requires an iterative solution. This is due to the need to convert between mole fraction and molal scales. The solution procedure is as follows:

1. Make initial guess for $m_{CO2,GUESS}$
2. $\gamma_x' = f(m_{CO2,GUESS})$
3. $x_{CO2} = f(\gamma_x')$
4. $m_{CO2,NEW} = f(x_{CO2})$

5. $\Delta = \left| m_{CO2,GUESS} - m_{CO2,NEW} \right|$
6. If $\Delta > tolerance, m_{CO2,GUESS} = m_{CO2,NEW}$, repeat from Step 2.

   If $\Delta < tolerance$, solution has converged

The methodology presented by Spycher and Pruess (21) is valid from 12-100°C, 1-600 bar and 0-6 molal NaCl concentration (21). However, the iterative procedure is slightly cumbersome for calculations.

3.5.4: Spycher and Pruess (21) adaptation of the method of Duan and Sun (25)

This methodology is a combination of models presented in Spycher et al. (27) and Duan and Sun (25) that is presented in Spycher and Pruess (21). If the CO_2 solubility model presented by Duan and Sun (25) is simplified into standard thermodynamic variables and the natural-log terms are eliminated, the following equation results (21):

$$m_{CO2} = \frac{F_{CO2}}{K_{CO2}\gamma_{CO2}} \qquad \text{Equation 36}$$

where F_{CO2} is the fugacity of the gaseous CO_2 phase, K_{CO2} is the thermodynamic equilibrium constant and γ_{CO2} is the activity coefficient of aqueous CO_2. Now assume there are two systems that are identical except that one consists of pure water and the other system consists of a brine solution with known ionic concentrations.

For pure water (21):

$$m^0_{CO2} = \frac{F_{CO2}}{K_{CO2}\gamma^0_{CO2}} \qquad \text{Equation 37}$$

For brine (21):

$$m_{CO2} = \frac{F_{CO2}}{K_{CO2}\gamma_{CO2}} \quad \text{Equation 38}$$

The gas phase fugacity and thermodynamic equilibrium constants are equal because they are functions of temperature and pressure but not salt content. Thus (21):

$$\frac{m^0_{CO2}}{m_{CO2}} = \frac{\gamma_{CO2}}{\gamma^0_{CO2}} \quad \text{Equation 39}$$

However, in pure water, γ_{CO2} approaches unity (16; 21; 27). Thus (21):

$$\frac{m^0_{CO2}}{m_{CO2}} = \gamma_{CO2} \quad \text{Equation 40}$$

Solving for m_{CO2} (21):

$$m_{CO2} = \frac{m^0_{CO2}}{\gamma_{CO2}} \quad \text{Equation 41}$$

To determine γ_{CO2}, the activity coefficient expression presented by Duan and Sun (25) is used (21), although it appears that any suitable method for estimating γ_{CO2} could suffice. To determine the solubility of CO_2 in pure water, ${m_{CO2}}^0$, the methodology presented by Spycher et al. (27) is used. This model is given by the following equation (27):

$$x^0_{CO2} = \frac{\Phi_{CO2}(1 - y_{H2O})P_{TOT}}{55.51K^0_{CO2(g)}} exp\left(\frac{-[P - P^0]\bar{V}}{RT}\right) \quad \text{Equation 42}$$

This model for determining solubility in pure water is identical to the model for determining CO_2 solubility (see Equation 32) in brine with the exception of the missing γ_x' term, which is neglected because γ_x' approaches unity in pure water (21). Eliminating the γ_x' term makes the solution procedure non-iterative because there is no conversion from mole fraction to molal scale. All other model parameters are calculated in an identical fashion to the procedure presented by Spycher and Pruess (21).

3.6: Summary

The parameters discussed in this chapter are used to describe the thermodynamic environment of a geochemical system. These parameters include solubility equilibrium constants for mineral precipitation and dissolution, for the formation of aqueous complexes, and for dissolution of CO_2. In addition, non-ideal effects due to high pressure, salinity, and temperature are accounted for using activity and fugacity coefficients. These parameters and their methods of estimation are then incorporated into the solution procedure discussed in Chapter 4 to describe pre- and post-injection conditions for CCS in a carbonate aquifer.

4: Model Development

4.1: Model Overview

Geochemical models are used to estimate the equilibrium concentrations of various dissolved ions for the purpose of quantifying mineral precipitation and dissolution in response to CO_2 injection. To accomplish this, models were developed to describe both pre-CO_2 injection and post-CO_2 injection geochemical conditions. For pre-injection conditions, the brine pH and salinity (salt mass-fraction) and the aquifer temperature and pressure are specified parameters and are used to estimate the initial equilibrium concentrations of dissolved ions. For post-injection conditions, CO_2 injection pressure, aquifer temperature and pressure, and brine salinity are specified parameters and are used to estimate the new equilibrium pH and ion concentrations. Then, the difference between pre- and post-injection equilibrium ion concentrations is used to estimate the extent of mineral precipitation and dissolution and net CO_2 solubility trapping that occurs during thermodynamic equilibrium processes associated with CO_2 injection.

4.2: System of Geochemical Equations

The geochemical model is used to solve for the equilibrium concentrations of 28 aqueous species, the activity of water, and the solution net charge. The geochemical system is non-linear, based on 30 equations and used to solve for 30 unknown values. This system of equations includes 24 equilibrium expressions for ions and aqueous

complexes, two total mass expressions for Na^+ and Cl^- ions, three equations to describe the dissociation and the activity of water, and one charge balance equation that calculates the net charge of the solution.

4.2.1: Rock Minerals

There are three solubility equilibrium expressions that describe the precipitation or dissolution of rock minerals assumed to be present in the aquifer. These rock minerals are calcite ($CaCO_{3(s)}$), dolomite ($CaMg(CO_3)_{2(s)}$), and gypsum ($CaSO_4 \cdot 2H_2O_{(s)}$). These three minerals are the sources of Ca^{2+}, Mg^{2+}, and SO_4^{2-} ions in solution that are available for geochemical reaction. The precipitation/dissolution reactions and log *K* values from the TOUGHREACT database (16) for each mineral are given in the following table:

Table 1: Equilibrium Reactions for Mineral Dissolution and Precipitation

	log *K*		
Reaction	35°C	45°C	55°C
Calcite $CaCO_{3(s)} + H^+ \overset{eq}{\Leftrightarrow} Ca^{2+} + HCO_3^-$	1.703	1.552	1.404
Dolomite $CaMg(CO_3)_{2(s)} + 2H^+ \overset{eq}{\Leftrightarrow} Ca^{2+} + Mg^{2+} + 2HCO_3^-$	2.173	1.828	1.492
Gypsum $CaSO_{4(s)} \cdot 2H_2O \overset{eq}{\Leftrightarrow} Ca^{2+} + SO_4^{2-} + 2H_2O$	-4.494	-4.533	-4.584

4.2.2: Carbonate System

There are three carbonate equilibrium expressions for $CO_{2(aq)}$, HCO_3^-, and CO_3^{2-} that take into account reactions of CO_2 in the aqueous phase and dissolution from the gaseous phase. For pre-injection conditions, the geochemical system is closed; i.e., there is no separate CO_2 gas phase that dissolved carbonate species must be in equilibrium with. Thus, the concentrations of aqueous carbonate species are constrained only by the assumed initial pH. For post-injection conditions, the geochemical system is open; i.e., the concentrations of aqueous carbonate species must be in equilibrium with a separate CO_2 phase that can dissolve into or out of solution. The carbonate system reactions and log *K* values from the TOUGHREACT database (16) are given in the following table:

Table 2: Equilibrium Reactions for Carbonate Species

Reaction	log *K*		
	35°C	45°C	55°C
$CO_{2(g,sc)} + H_2O \overset{eq}{\Leftrightarrow} H^+ + HCO_3^-$	-7.875	-7.945	-8.018
$CO_{2(aq)} + H_2O \overset{eq}{\Leftrightarrow} H^+ + HCO_3^-$	-6.297	-6.273	-6.267
$CO_3^{2-} + H^+ \overset{eq}{\Leftrightarrow} HCO_3^-$	10.249	10.191	10.148

Note that that equilibrium relationship for $CO_{2(g,sc)}$ and HCO_3^- in Table 2 is not used when other methods (i.e., Duan and Sun (25) or Spycher and Pruess (21)) are used to estimate the molal concentration of $CO_{2(aq)}$, m_{CO2}. In this case, m_{CO2} is estimated using other methods and the equilibrium relationship between $CO_{2(aq)}$ and HCO_3^- is assumed to be valid for remaining calculations.

4.2.3: Aqueous Complexes

There are 18 equilibrium expressions that describe aqueous-complexing reactions that are combinations of the ions in solution made available by the previous six equilibrium reactions given in Table 1 and Table 2. These aqueous complexes include both dissolved charged species ($CaCl^+$, $MgHCO_3^+$, $NaSO_4^-$, etc) and dissolved neutral species ($NaCl_{(aq)}$, $NaHCO_{3(aq)}$, etc). The following table contains the 18 aqueous-complexing reactions considered and their respective log *K* values from the TOUGHREACT database (16).

Table 3: Equilibrium Reactions for Aqueous Complexes

Reaction	log *K*		
	35°C	45°C	55°C
$CaCl^+ \overset{eq}{\Leftrightarrow} Ca^{2+} + Cl^-$	0.682	0.650	0.610
$CaCl_{2(aq)} \overset{eq}{\Leftrightarrow} Ca^{2+} + 2Cl^-$	0.673	0.668	0.643
$CaCO_{3(aq)} + H^+ \overset{eq}{\Leftrightarrow} Ca^{2+} + HCO_3^-$	6.834	6.671	6.520
$CaHCO_3^+ \overset{eq}{\Leftrightarrow} Ca^{2+} + HCO_3^-$	-1.060	-1.092	-1.135
$CaOH^+ + H^+ \overset{eq}{\Leftrightarrow} Ca^{2+} + H_2O$	12.486	12.141	11.816
$CaSO_{4(aq)} \overset{eq}{\Leftrightarrow} Ca^{2+} + SO_4^{2-}$	-2.140	-2.188	-2.241
$HCl_{(aq)} \overset{eq}{\Leftrightarrow} H^+ + Cl^-$	0.697	0.688	0.676
$HSO_4^- \overset{eq}{\Leftrightarrow} H^+ + SO_4^{2-}$	-2.101	-2.188	-2.373
$MgCl^+ \overset{eq}{\Leftrightarrow} Mg^{2+} + Cl^-$	0.133	0.111	0.075
$MgCO_{3(aq)} + H^+ \overset{eq}{\Leftrightarrow} Mg^{2+} + HCO_3^-$	7.220	7.094	6.978
$MgHCO_3^+ \overset{eq}{\Leftrightarrow} Mg^{2+} + HCO_3^-$	-1.054	-1.090	-1.137
$MgOH^+ + H^+ \overset{eq}{\Leftrightarrow} Mg^{2+} + H_2O$	11.434	11.105	10.796

Reaction	log *K*		
	35°C	45°C	55°C
$MgSO_{4(aq)} \overset{eq}{\Leftrightarrow} Mg^{2+} + SO_4{}^{2-}$	-2.510	-2.645	-2.781
$NaCl_{(aq)} \overset{eq}{\Leftrightarrow} Na^{+} + Cl^{-}$	0.749	0.711	0.670
$NaCO_3{}^{-} + H^{+} \overset{eq}{\Leftrightarrow} Na^{+} + HCO_3{}^{-}$	9.864	9.935	10.027
$NaHCO_{3(aq)} \overset{eq}{\Leftrightarrow} Na^{+} + HCO_3{}^{-}$	-0.085	-0.001	0.081
$NaOH_{(aq)} + H^{+} \overset{eq}{\Leftrightarrow} Na^{+} + H_2O$	13.850	13.575	13.325
$NaSO_4{}^{-} \overset{eq}{\Leftrightarrow} Na^{+} + SO_4{}^{2-}$	-0.840	-0.870	-0.899

4.2.4: Salinity

It is assumed that the salinity (salt mass fraction) is a known parameter, and the salt mass fraction is considered to be only NaCl. The contribution to salinity due to other dissolved ions is assumed to be insignificant. Thus, the total mass of Na^+ and Cl^- available for reaction per unit volume is specified by the assumed salinity. Salinity, *S*, is defined by the following equation:

$$S = \frac{mass\ \ NaCl}{mass\ \ NaCl + mass\ H_2O} \times 100\% \ = \ \frac{mass\ \ NaCl}{mass\ Brine} \times 100\% \qquad \text{Equation 43}$$

where *S* is in percent. This is used to specify the total molal concentration of Na^+ and Cl^- ions:

$$\left(m_{Na,Cl}\right)_{TOT} = \frac{S}{MW_{NaCl} \times (1 - S)} \qquad \text{Equation 44}$$

where $(m_{Na,Cl})_{TOT}$ is the total molal concentration of Na^+ and Cl^- ions respectively, and

MW_{NaCl} is the formula weight for NaCl ($58.443*10^{-3}$ kg/mole). Note that this equation is applied twice in the geochemical model to determine the concentrations of both Na^+ and Cl^-. This is used as a constraint for all species containing Na^+ and Cl^- because the sum of concentration of Na^+ and Cl^- in all species containing Na^+ and Cl^- must equal the total concentrations for Na^+ and Cl^- specified by the known salt mass-fraction.

4.2.5: Water (H_2O) System

The dissociation of water (H_2O) into H^+ and OH^- ions must be considered for any system contained within the aqueous phase. The water dissociation reaction and log *K* values from the TOUGHREACT database (16) are given in the following table:

Table 4: Equilibrium Reactions for H_2O Dissociation

	log *K*		
Reaction	35°C	45°C	55°C
$H^+ + OH^- \overset{eq}{\Leftrightarrow} H_2O$	13.680	13.400	13.146

The activities of H^+ and OH^- are related to the activity of H_2O (see Chapter 3.4) by the following expression:

$$K_W = \frac{a_{H2O}}{a_{H^+} * a_{OH^-}} \qquad \text{Equation 45}$$

The pH of the brine is related to the chemical activity of H^+ by the following equation:

$$pH = -\log a_{H^+} \qquad \text{Equation 46}$$

4.2.6: Charge Balance

The charge balance equation quantifies the net charge of the solution. It is the sum of the concentrations all ionic and complexed species multiplied by their respective overall charge:

$$NET\ CHARGE = \sum_j m_j z_j + \sum_q m_q z_q \qquad \text{Equation 47}$$

where m indicates molal concentration, z indicates charge, subscript j indicates ions and subscript q indicates aqueous complexes.

4.3: Iterative Solution Procedure

Because the system of equations is non-linear, an iterative solution procedure is required. In this iterative procedure, a basis species from the parent reactions that appears often in the system of equilibrium equations is chosen. The basis species is chosen in such a way that all other geochemical species are functions of this species and its value can be conveniently iterated until all equations are satisfied. Essentially, this means picking a basis species that is not specified by any known parameters. The molal concentration of this basis species is then iterated until the net solution charge converges to zero (within an allowable tolerance). For initial conditions (pre-injection), the basis species is bicarbonate ion, HCO_3^-, because it is not constrained solely by any specified parameter (i.e. initial pH, aquifer pressure, salinity, or temperature). For calculations after CO_2 injection occurs, H^+ is the chosen basis species because the pH is no longer specified and the activity of HCO_3^- is now constrained by equilibrium with the gaseous CO_2 phase. The solution procedure consists of an inner iteration loop and an outer iteration loop which are discussed below.

4.3.1: Inner Iteration Loop

The purpose of the inner iteration loop is to estimate concentrations of all geochemical species given a particular starting estimate for the concentration of the basis species. The inner iteration loop is necessary because thermodynamic parameters like activity coefficients, activity of water, and aqueous CO_2 concentration are functions of the concentrations of all geochemical species, which are functions of thermodynamic parameters and the concentration of the basis species. Figure 5 and Figure 6 are flow charts of the algorithms used for the inner iteration loop for pre- and post-injection conditions, respectively.

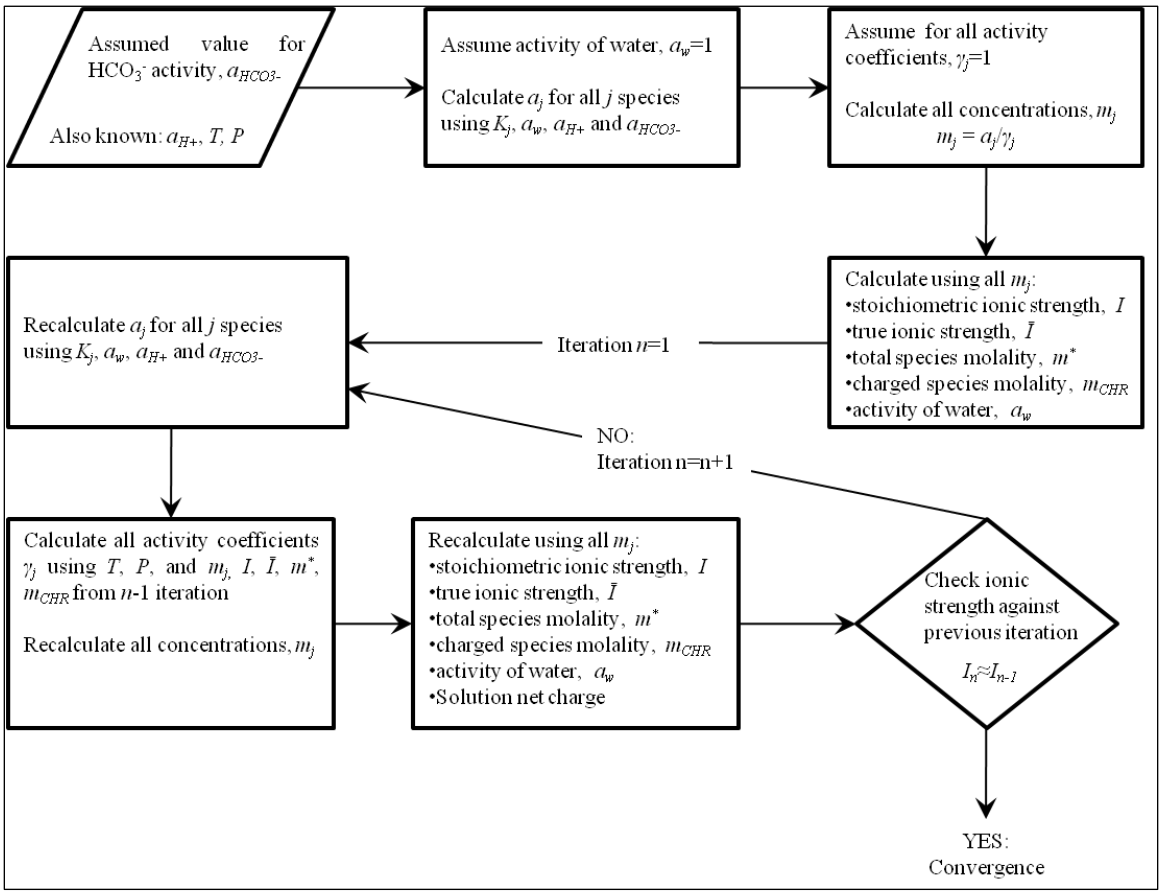

Figure 5: Inner Iteration Loop for Pre-CO_2 Injection

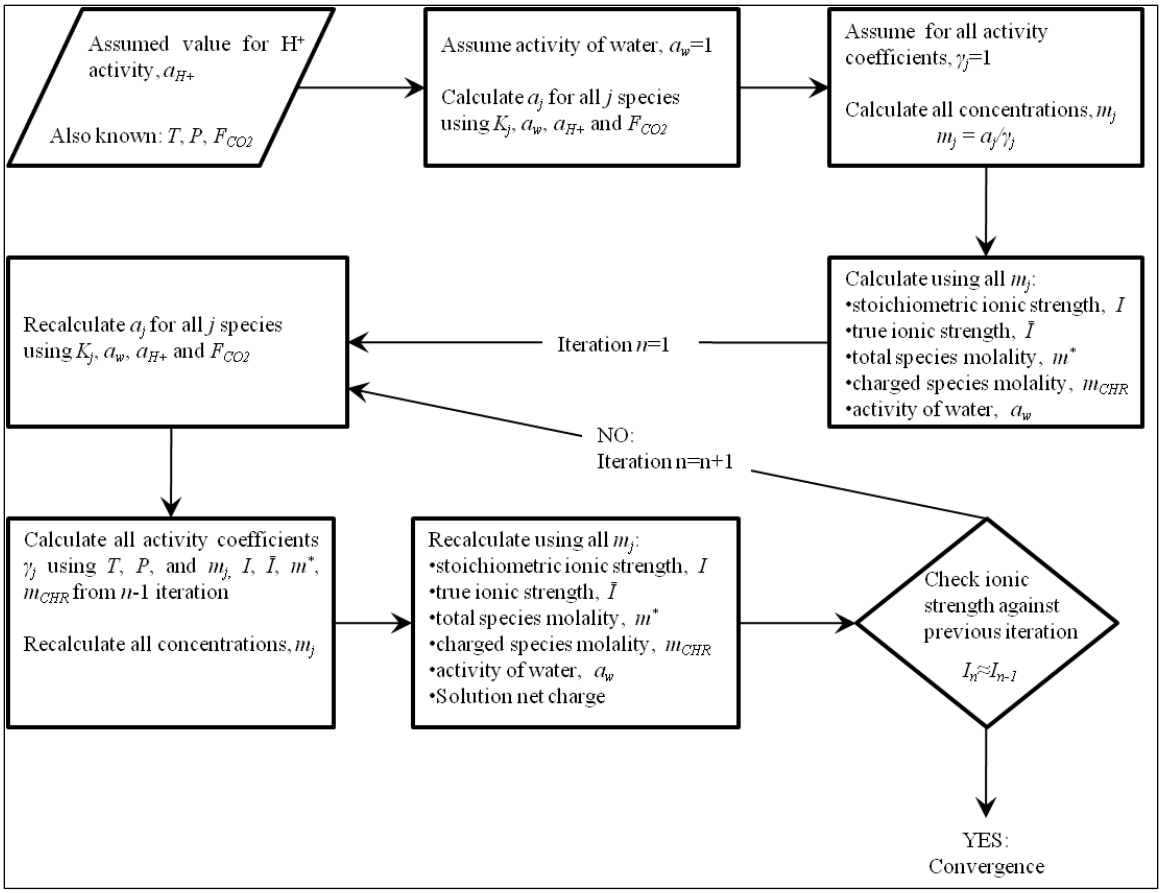

Figure 6: Inner Iteration Loop for Post-CO_2 Injection

In order to generate initial estimates for the activities and molal concentrations of all geochemical species, activity coefficients are initially assumed to equal unity. The initial estimates for activities and molal concentrations are then used to initialize the inner iteration loop. The molal concentrations of species *j* at iteration *n* are solved for using the following expression:

$$(a_j)_n = \frac{\prod(a_{\neq j})_{n-1}^{\nu}}{K_j} \qquad \text{Equation 48}$$

where $a_{\neq j}$ is the activity of all other species in the j^{th} equilibrium reaction raised to their

respective stoichiometric coefficient v, and K_j is the equilibrium constant for the j^{th} equilibrium reaction (as given in Tables 1-4).

The activity of species j is used to estimate the concentration of species j at iteration n with the following expression:

$$(m_j)_n = \frac{(a_j)_n}{(\gamma_j)_n} \quad \text{Equation 49}$$

where γ_j is the activity coefficient for species j. The activity coefficient for the j^{th} ion at iteration n is estimated using concentrations and the ionic strength from the previous iteration:

$$(\gamma_j)_n = f(T, P, z, m_{n-1}, I_{n-1}) \quad \text{Equation 50}$$

The procedure is similar for estimating the activity of water at the n^{th} iteration:

$$(a_W)_n = f(T, P, z_j, m_{n-1}, I_{n-1}) \quad \text{Equation 51}$$

To solve for the concentrations of free Na^+ and Cl^- ions at iteration n, the following expressions are used:

$$(m_{Na^+})_n = (m_{Na^+})_{TOTAL} - \left(\sum_q \nu_{Na+} (m_{Na^+})_q \right)_{n-1} \quad \text{Equation 52}$$

$$(m_{Cl^-})_n = (m_{Cl^-})_{TOTAL} - \left(\sum_q \nu_{Cl-} (m_{Cl^-})_q \right)_{n-1} \quad \text{Equation 53}$$

where m indicates molal concentration and $(m_{Na+})_q$ and $(m_{Cl-})_q$ indicate molal concentration of Na^+ and Cl^- in aqueous complex q multiplied by their stoichiometric coefficient v, respectively. These concentrations for free Na^+ and Cl^- ions are then used to solve for the activities of aqueous complexes containing Na^+ and Cl^- ions for iteration n.

The inner iteration loop is considered to have converged when the change in ionic strength between successive iterations is less than a specified tolerance. A minimal change in ionic strength between iterations indicates that a stable solution has been determined for the given basis species activity.

4.3.2: Outer Iteration Loop

At equilibrium, the solution cannot have a net charge. Thus, the model is solved in such a way as to drive the net charge of the brine to zero, and the charge balance equation is used as the convergence criterion for the outer iteration process. An initial estimate is made for the concentration of the basis species and the inner iteration loop is solved to convergence. Then, the outer iteration loop is used to iterate the concentration of the basis species until the calculated solution charge approaches zero (within a specified tolerance). Figure 7 is a flowchart demonstrating the algorithm used for the outer iteration loop. For each iteration of the outer loop, a new value for the pH (pre-injection) or $[HCO_3^-]$ (post-injection) is tested. For each value of pH or $[HCO_3^-]$ tested, the inner iteration loop must be solved to convergence. When the solution net charge approaches zero, the system has converged and the model yields the equilibrium concentrations of the geochemical species.

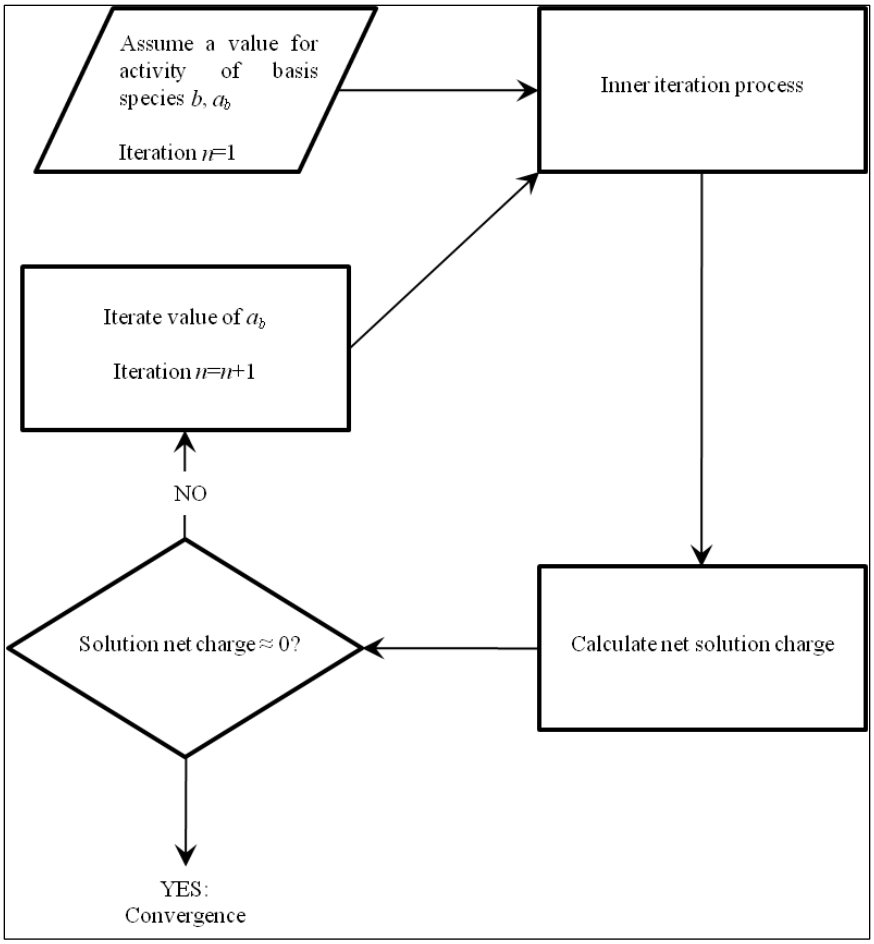

Figure 7: Outer Iteration Loop

4.4: Model Implementation

Computer programs were developed to calculate activity coefficients for ionic species, charged aqueous complexes, and aqueous CO_2; the fugacity coefficient for $CO_{2(g,sc)}$; aqueous CO_2 concentration; and the activity of water. These programs are written in Visual Basic so they can be implemented in a Microsoft Excel spreadsheet where inner and outer iterative calculations are performed.

The inner iteration loop is written directly into the spreadsheet as sequential blocks of cells where calculations are carried out and relevant values are passed forward to the next block. In practice, a fixed number of inner iterations are written explicitly into the

structure of the spreadsheet. Excess iterations are written into the spreadsheet to ensure that the inner loop will converge for a given estimate of the basis species concentration. In most cases, fewer than ten inner iterations are required per outer iteration, and 20 inner iterations are sufficient in all scenarios examined. The outer loop is iterated using the SOLVER function that is included in Microsoft Excel. The SOLVER function iterates the concentration of the basis species until the convergence criterion of net solution charge approaching zero is met.

4.5: Model Limitations

The geochemical model is based on the assumption of system equilibrium for both pre- and post-CO_2 injection conditions. The model only examines geochemistry in the residual brine saturation and does not address chemical processes that occur at the moving CO_2-brine interface. The model also assumes the presence of only three minerals: calcite, dolomite, and gypsum. The model is based on the assumption that only these three minerals are allowed to dissolve and/or precipitate. Finally, the model does not address advective/transport effects or chemical reaction rates.

4.6: Model Outputs

Once solved, the geochemical model yields the concentrations and activity coefficients of all aqueous species included in the system, the activity of water, and the $CO_{2(g,sc)}$ fugacity for post-injection conditions. Next, the amount of minerals that precipitate or dissolve due to CO_2 injection can be estimated by examining the difference in concentrations of calcium, magnesium, and sulfate ions in solution for pre- and post-injection conditions. Positive concentration difference indicates that ions enter solution

due to mineral dissolution, and negative concentration difference indicates that ions leave solution due to mineral precipitation. Thus:

$$\Delta Dolomite = \left(m_{Mg^{2+}}\right)_{post} - \left(m_{Mg^{2+}}\right)_{pre} \quad \text{Equation 54}$$

$$\Delta Gypsum = \left(m_{SO_4^{2-}}\right)_{post} - \left(m_{SO_4^{2-}}\right)_{pre} \quad \text{Equation 55}$$

$$\Delta Calcite = \left[\left(m_{Ca^{2+}}\right)_{post} - \left(m_{Ca^{2+}}\right)_{pre}\right] - \Delta Dolomite - \Delta Gypsum \quad \text{Equation 56}$$

where *m* indicates molal concentration and subscripts *pre* and *post* refer to conditions before and after CO_2 injection, respectively.

Changes in concentrations of carbonate species can also be used to estimate the net CO_2 storage via the solubility trapping mechanism:

$$\begin{aligned} Net\ CO_2\ Storage &= \left(\sum carbonate\ species\right)_{post} \\ &- \left(\sum carbonate\ species\right)_{pre} \\ &- (\Delta Calcite + 2 \times \Delta Dolomite) \end{aligned} \quad \text{Equation 57}$$

4.7: Comparison of Thermodynamic Sub-models

With three different models for estimating γ_{CO2}, two models for estimating φ_{CO2}, and four models for estimating m_{CO2}, as described in Chapter 3, there are 24 possible combinations of thermodynamic sub-models that could be studied. Initially, nine overall geochemical models were developed using different combinations of the thermodynamic models, as summarized in Table 5.

Table 5: Combinations of Sub-Models for CO_2 Thermodynamic Parameter Estimation

Model	Sub-models for CO_2 thermodynamic parameter estimation		
	$CO_{2(aq)}$ Activity Coefficient	$CO_{2(g,sc)}$ Fugacity Coefficient	$CO_{2(aq)}$ Solubility
1	Drummond (22)	Spycher and Reed (26)	Equilibrium Constant (16)
2	Drummond (22)	Duan and Sun (20)	Equilibrium Constant (16)
3	Rumpf et al. (23)	Duan and Sun (20)	Equilibrium Constant (16)
4	Rumpf et al. (1994)	Spycher and Reed (20)	Equilibrium Constant (16)
5	Duan and Sun (2003)	Duan et al. (20)	Duan and Sun (25)
6	Drummond (22)	Duan et al. (20)	Duan and Sun (25)
7	Drummond (22)	Duan et al. (20)	Spycher and Pruess (21) adaptation of Duan and Sun (25)
8	Rumpf et al. (23)	Duan et al. (20)	Spycher and Pruess (21)
9	Rumpf et al. (23)	Spycher and Reed (26)	Spycher and Pruess (21)

These nine combinations of thermodynamic sub-models were then used to examine a baseline geochemical scenario to determine the sensitivity of model outputs to the choice of thermodynamic sub-models. The baseline geochemical scenario has an initial pH of 7.5, brine salinity of 10%, initial aquifer pressure of 100 bar, CO_2 injection pressure of 160 bar, and aquifer temperature of 45°C. The equilibrium pH, equilibrium CO_2 molality, and mineral precipitation/dissolution for calcite, dolomite and gypsum were determined for each model after CO_2 injection and plotted along with their respective average values in the following figures:

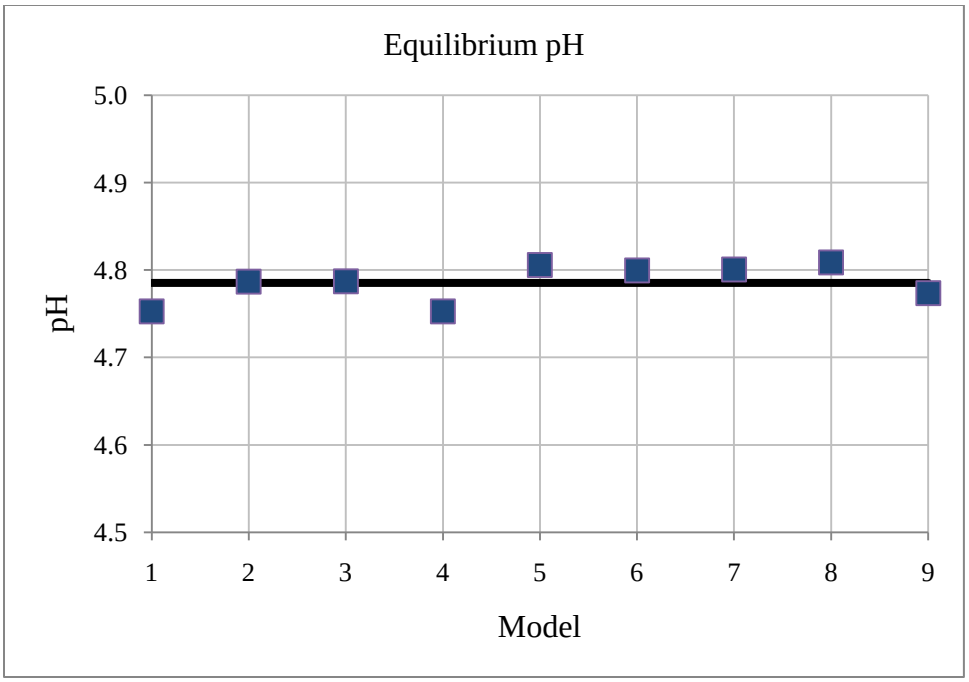

Figure 8: Equilibrium pH for Various Choices of Thermodynamic Sub-Models

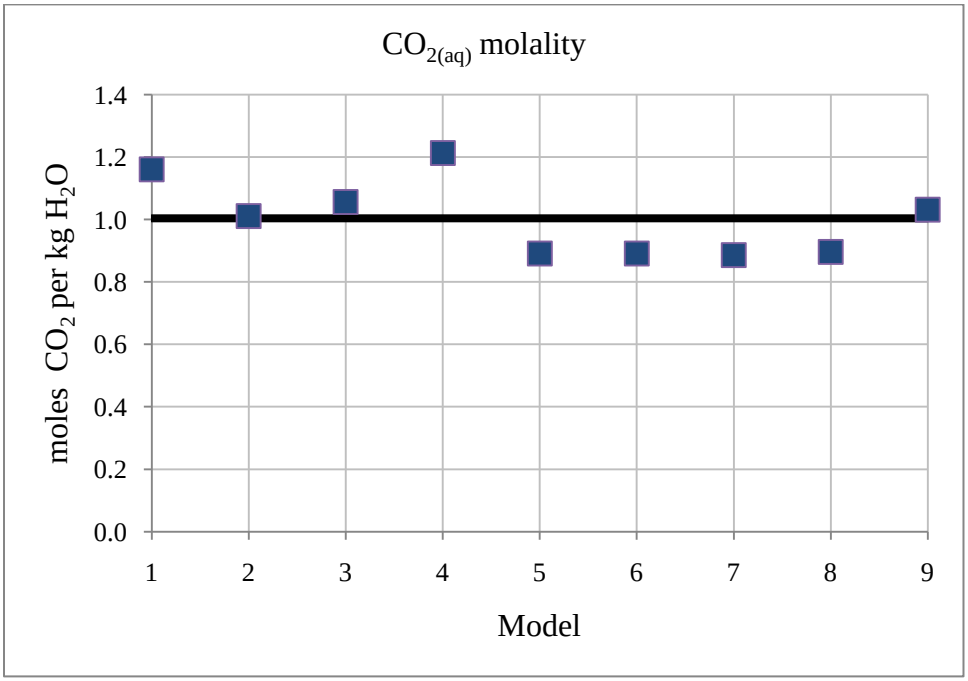

Figure 9: CO_2 Molality for Various Choices of Thermodynamic Sub-Models

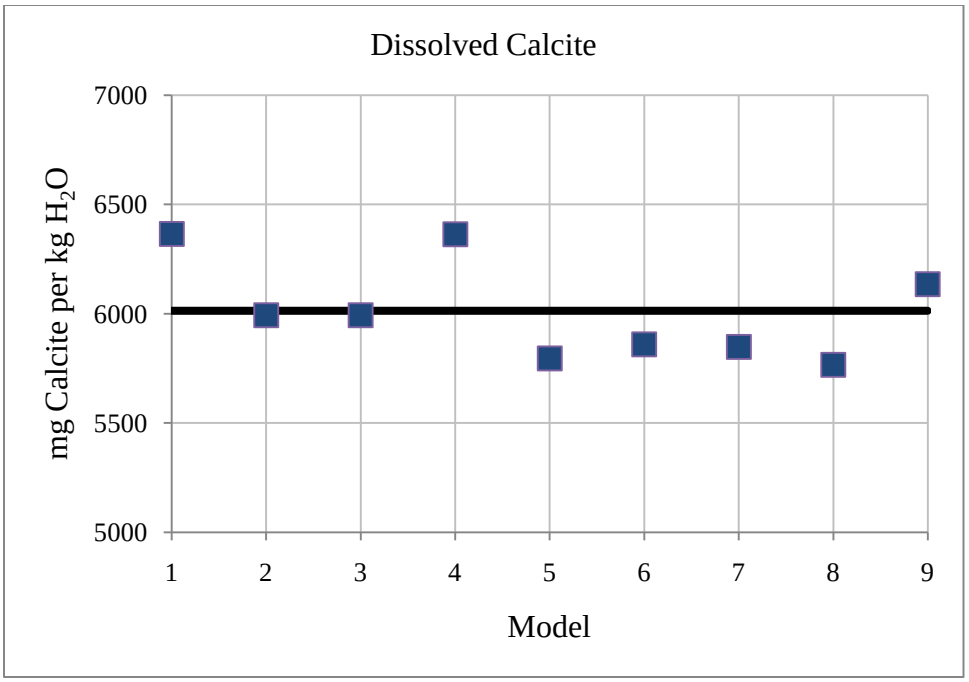

Figure 10: Calcite Dissolution for Various Choices of Thermodynamic Sub-Models

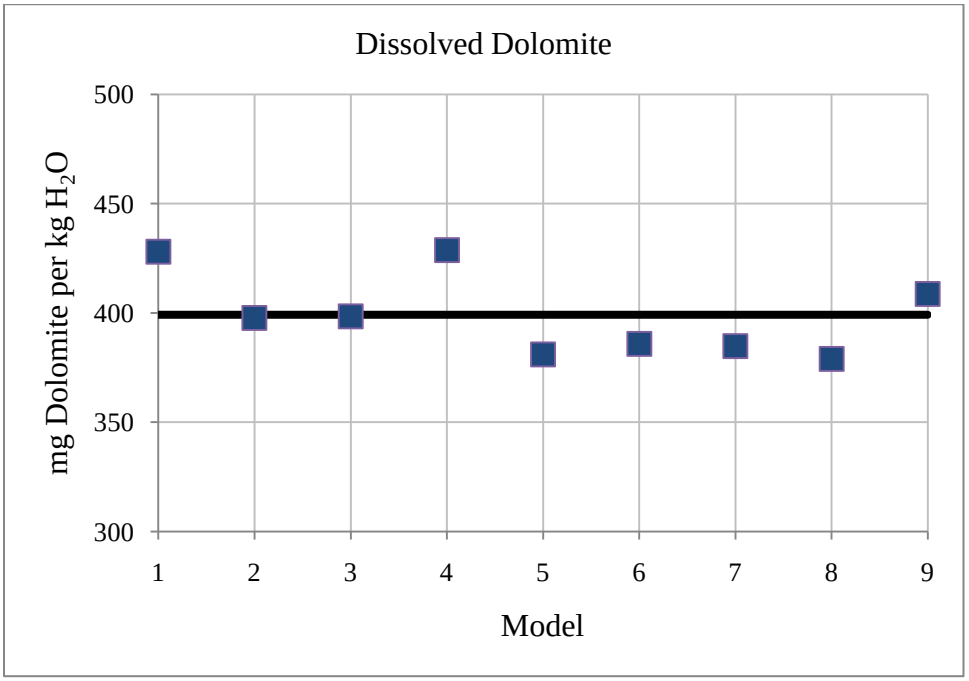

Figure 11: Dolomite Dissolution for Various Choices of Thermodynamic Sub-Models

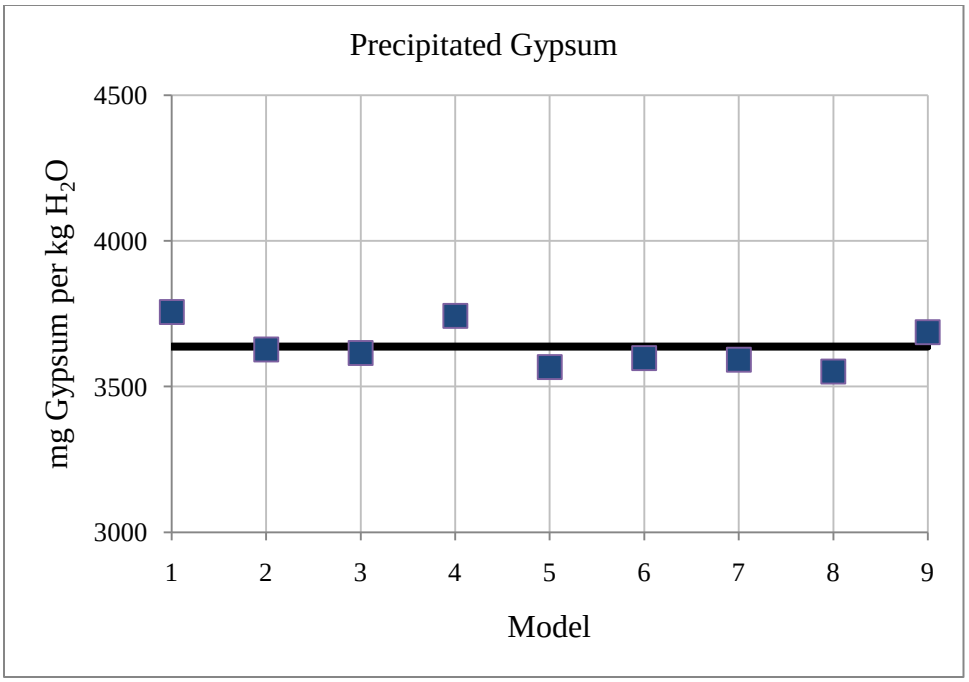

Figure 12: Gypsum Precipitation for Various Choices of Thermodynamic Sub-Models

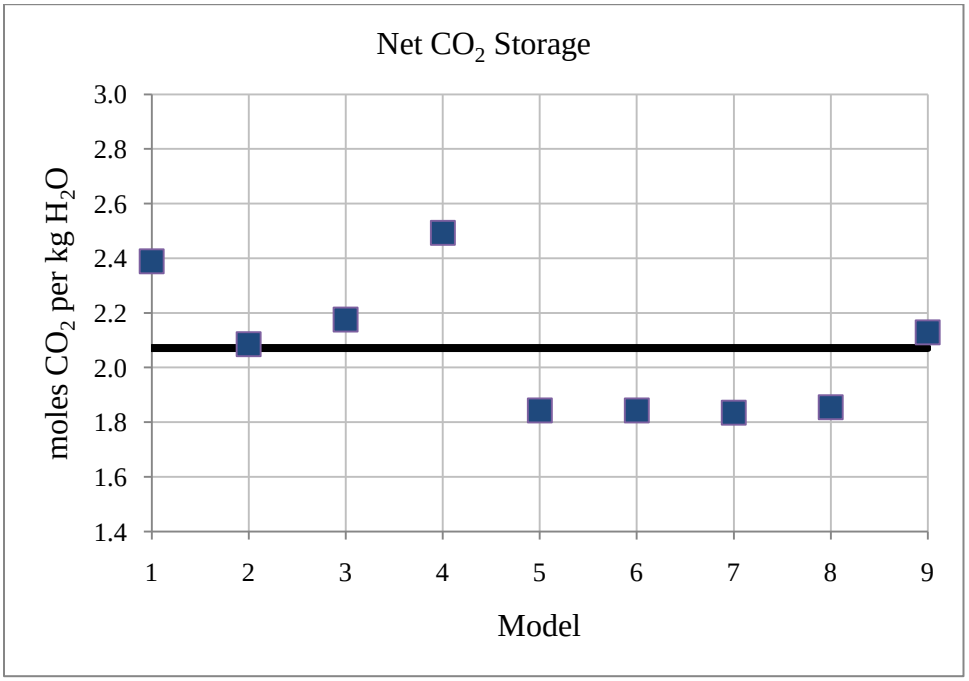

Figure 13: Net CO_2 Storage for Various Choices of Thermodynamic Sub-models

The average equilibrium pH is around 4.79, and this agrees closely with results in the literature (5; 7). The average CO_2 concentration is 1.0 molal, which also agrees generally well with results by others (5; 7). In general, the different combinations of thermodynamic models yield similar results. Precipitation of gypsum and dissolution of calcite and dolomite also agree well with predictions by others (5; 7). The average estimated net CO_2 storage is around 2.1 molal.

Several trends can be observed based on the choices of CO_2 parameter sub-models. First, the choice of methodology for estimating the activity coefficient for $CO_{2(aq)}$ does not have significant effect on the model predictions. Next, it is observed that systems using the equilibrium constant from the thermodynamic database for calculating the concentration of $CO_{2(aq)}$ (i.e., models 1-4) predict higher values for mineral precipitation and dissolution, $CO_{2(aq)}$ concentration, and net CO_2 storage than systems using the Duan and Sun (25) or the Spycher and Pruess (21) solubility models (i.e., models 5-9). This is because the equilibrium constant method for estimating CO_2 solubility does not take into account the effects of high ionic strength, and probably over-estimates the dissolved CO_2 concentration. In general, the models using more recent correlations for CO_2 solubility that include the effects of dissolved ions (models 5-9) are in good agreement.

Using the CO_2 fugacity model as a distinguishing characteristic, it is observed that models using the Spycher and Reed (26) model for $CO_{2(g,sc)}$ fugacity coefficient (i.e., models 1, 4, and 9) estimate higher values for mineral dissolution/precipitation, $CO_{2(aq)}$ concentration, and net CO_2 storage, and estimate lower values for equilibrium pH. The choice of fugacity coefficient model has the greatest effect on geochemical predictions. This is because the temperatures and pressures being considered are at the low end of the

recommended ranges for use with the Spycher and Reed model where inaccuracies are reported for fugacity coefficient estimation (26). The fugacity coefficient model presented by Duan et al. (20) is fitted to experimental data for six different *T-P* regimes and probably a better choice for the conditions considered.

However, the differences in geochemical predictions are generally low – estimates from all models for the equilibrium pH agree to within ±1% of the average, estimates from all models for mineral precipitation and dissolution agree to within ±10% of the average, and estimates from all models for m_{CO2} and net CO_2 storage agree to within ±25% of the average. This suggests that the choice of thermodynamic sub-models for estimating CO_2 parameters does not have a large effect on the solution to the geochemical system. Additionally, these results suggest that variations in estimated CO_2 solubility have a limited effect on other estimated quantities like equilibrium pH and mineral precipitation or dissolution.

From these nine geochemical systems, three were chosen such that each model used different sub-models for calculating m_{CO2} and γ_{CO2}. The models chosen for further investigation are models 1, 5, and 8 from the preceding table. These models are used to examine the sensitivity of the system to key chemical and physical parameters as described in the next chapter.

5: Model Results

Models 1, 5 and 8 are used to examine the effects of initial pH, CO_2 injection pressure, salinity, and temperature on the geochemical system. Simulations are performed such that one parameter varies while the other three are kept constant in order to evaluate the sensitivity of the geochemical system to the varying parameter. These simulations are variants of the base case described in Chapter 4 where the initial pH is 7.5, aquifer pressure is 100 bar, CO_2 injection pressure is 160 bar, salinity is 10%, and temperature is 45°C.

5.1: Effect of Initial pH

In these simulations, temperature, CO_2 injection pressure and salinity are constant at 45°C, 160 bar and 10%, respectively. Three sets of simulations using an initial pH of 6.5, 7.5, and 8.5 were performed.

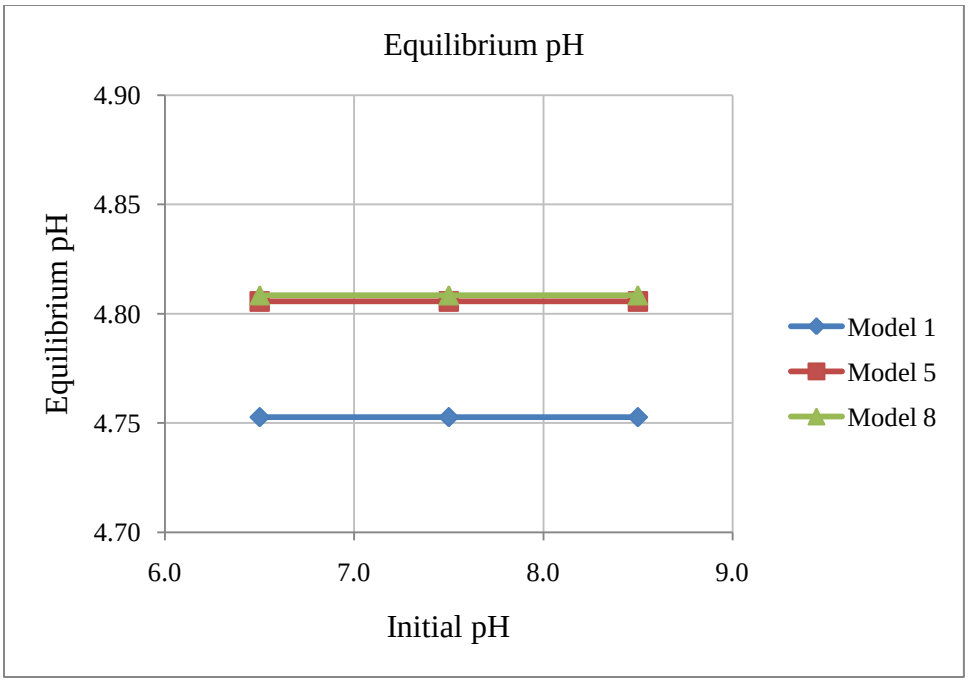

Figure 14: Equilibrium pH as a Function of Initial pH

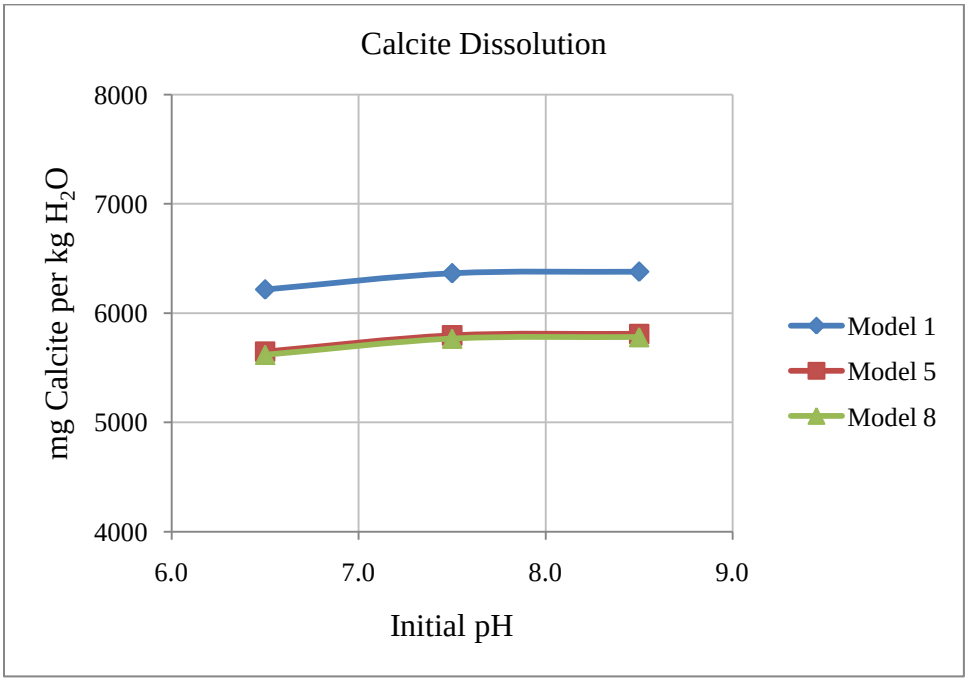

Figure 15: Calcite Dissolution as a Function of Initial pH

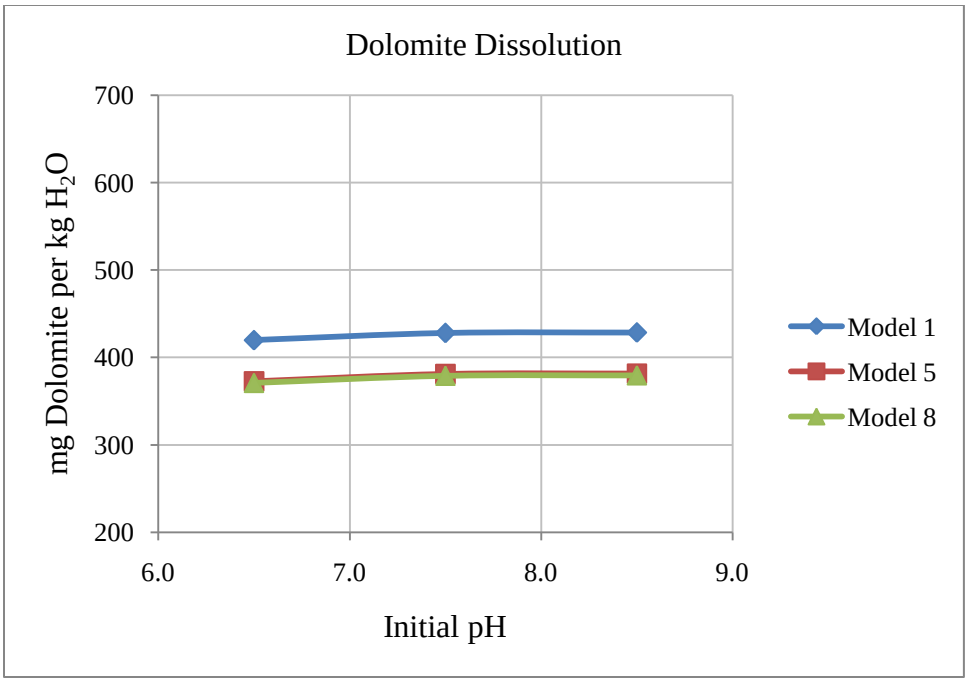

Figure 16: Dolomite Dissolution as a Function of Initial pH

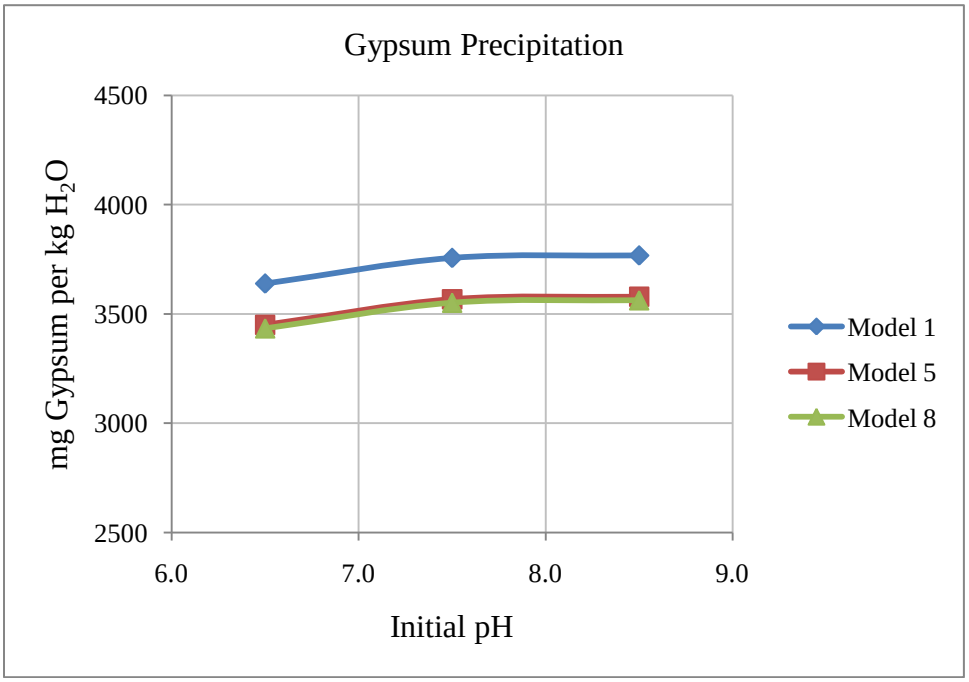

Figure 17: Gypsum Precipitation as a Function of Initial pH

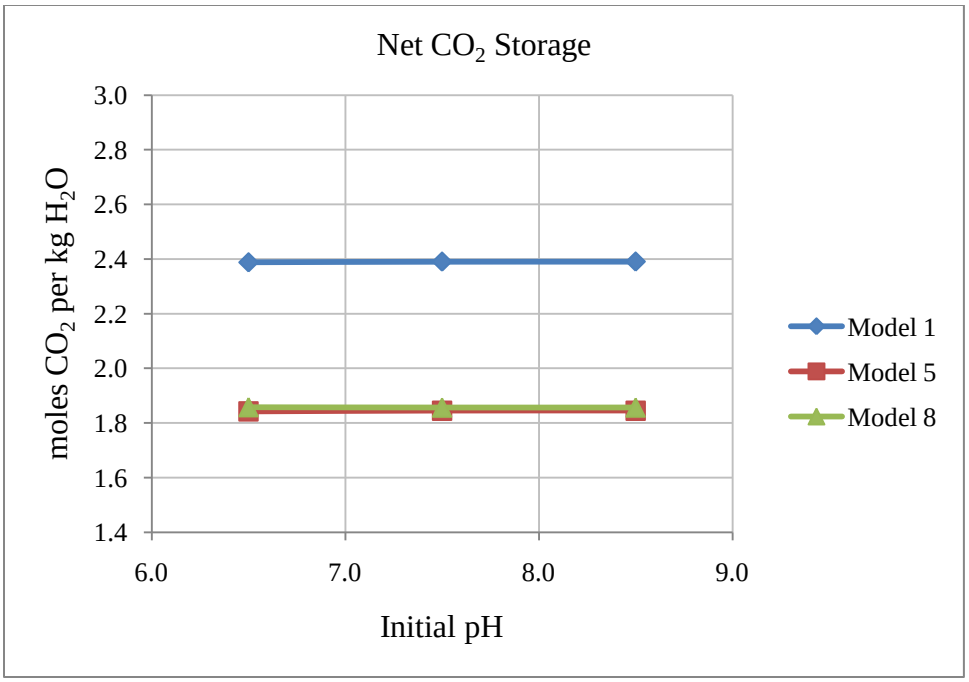

Figure 18: Net CO_2 Storage as a Function of Initial pH

Note that the geochemical system predicts slightly increasing quantities for mineral dissolution and precipitation and very slightly increasing net CO_2 storage with increasing initial pH. However, the system is insensitive to initial pH. This is consistent with the findings by others (7). Insensitivity to initial pH is due to the fact that equilibrated pre-injection brine has similar composition over the range of pH examined due to the dominance of bicarbonate ion in solution for pH 6-9. Note also that the initial pH has no effect on the equilibrium pH for post-CO_2 injection conditions. The initial pH does not influence the equilibrium pH after CO_2 injection because the post-injection system has excess CO_2 available, so the separate CO_2 phase will be the controlling phase for equilibrium. Because of these reasons, net mineral precipitation and dissolution is influenced very little by the initial pH.

5.2: Effect of CO_2 Injection Pressure

In these simulations, temperature, initial pH and salinity are constant at 45°C, 7.5 and 10%, respectively. Three sets of simulations are performed for CO_2 injection pressures of 120, 160 and 200 bars.

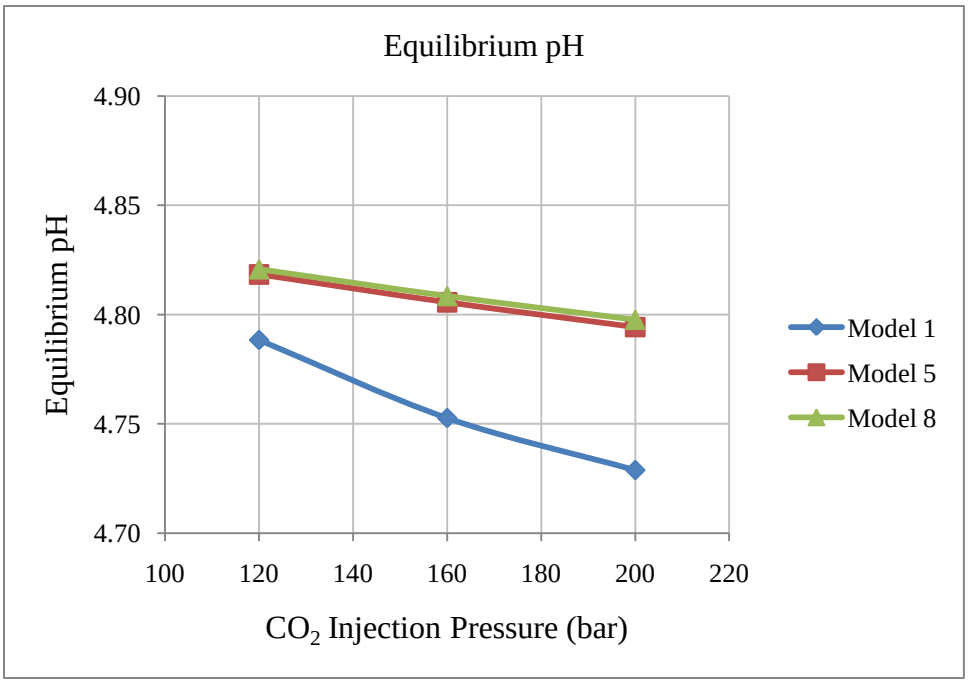

Figure 19: Equilibrium pH as a Function of CO_2 Injection Pressure

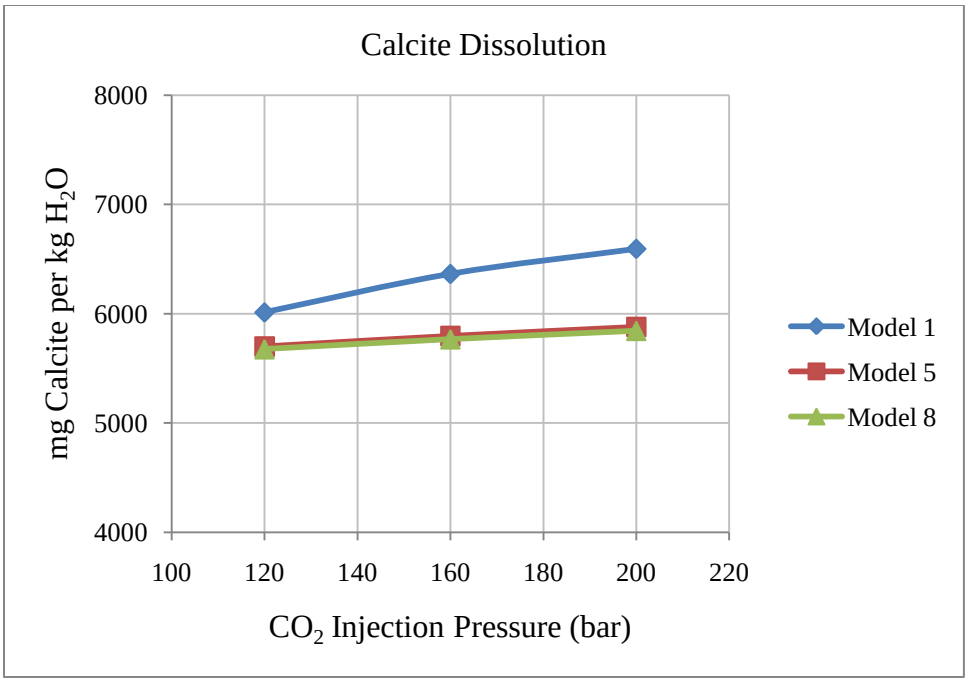

Figure 20: Calcite Dissolution as a Function of CO_2 Injection Pressure

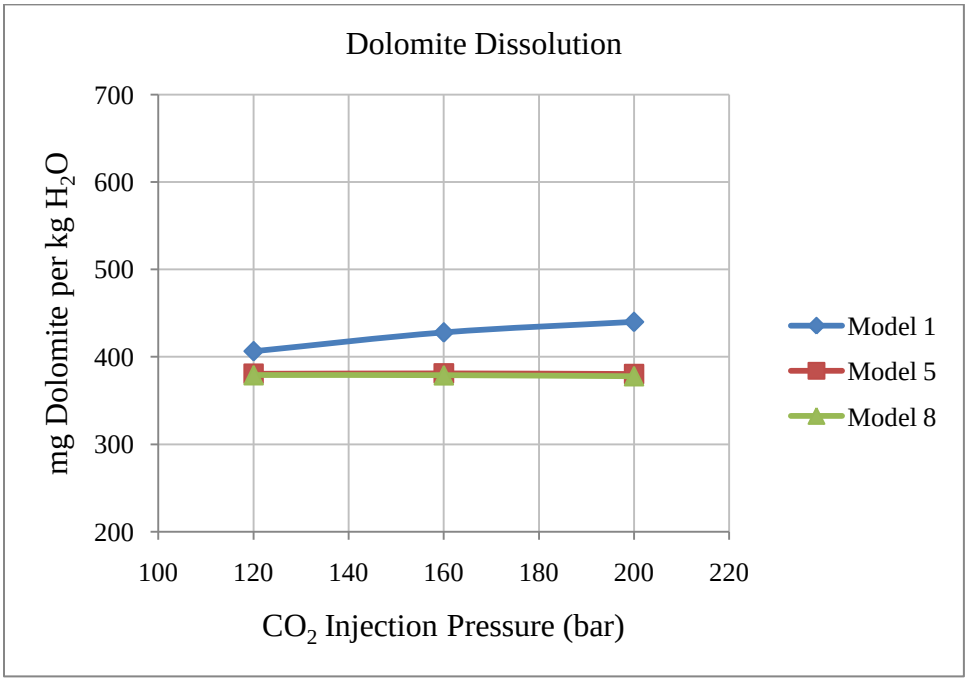

Figure 21: Dolomite Dissolution as a Function of CO_2 Injection Pressure

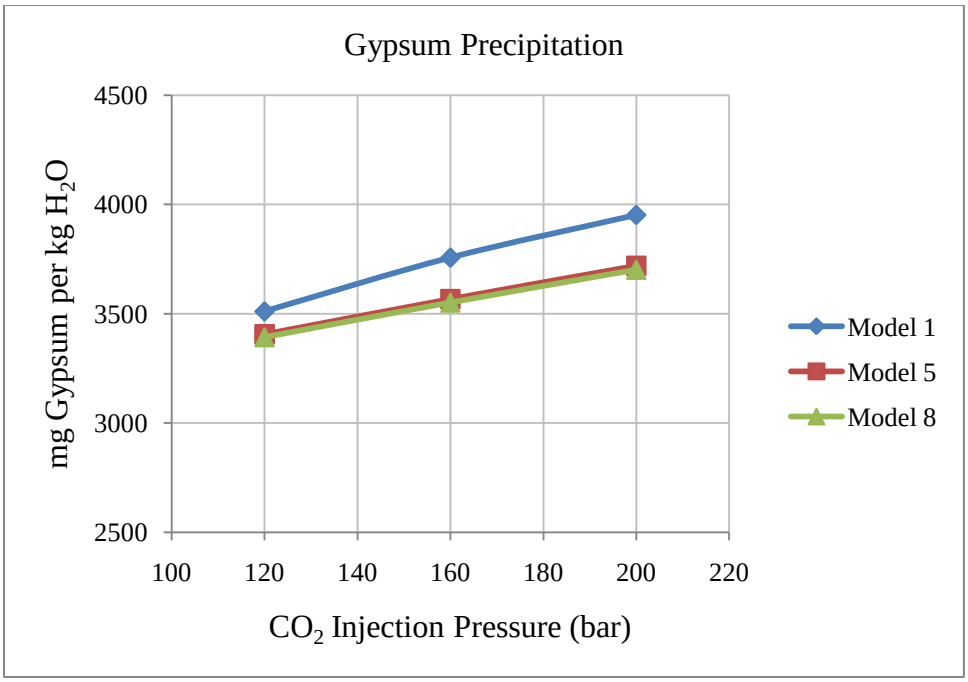

Figure 22: Gypsum Precipitation as a Function of CO_2 Injection Pressure

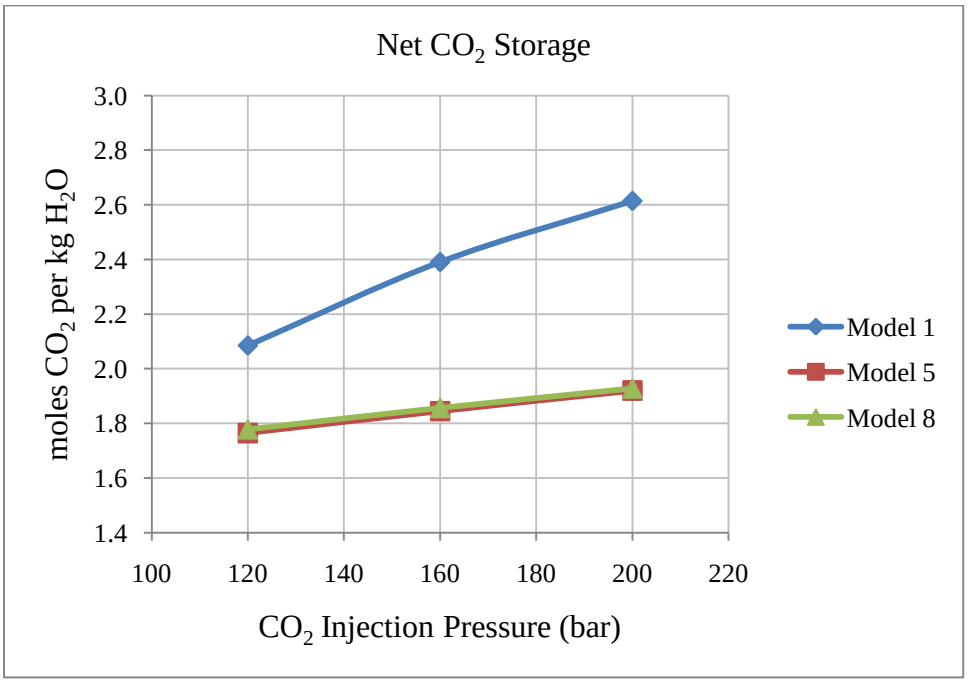

Figure 23: Net CO_2 Storage as a Function of CO_2 Injection Pressure

Note that the geochemical system predicts slightly increasing quantities of mineral dissolution and precipitation, decreased equilibrium pH, and increased net CO_2 storage in response to increasing CO_2 injection pressure. However, the system is relatively insensitive to CO_2 injection pressure. This is due to the fact that the fugacity of the $CO_{2(g,sc)}$ phase does not vary proportionally with pressure over the range of pressures examined. Using the baseline scenario and the Spycher and Reed (26) methodology for estimating CO_2 fugacity, varying the pressure from 120 bar to 200 bar results in a change in fugacity from 70 to 88 bar; i.e. a 67% increase in pressure results in a 26% increase in fugacity. Similarly, using the Duan et al. (20) methodology for estimating CO_2 fugacity, the same 67% increase in pressure results in a 19% increase in CO_2 fugacity. This minimizes the effects of increased CO_2 pressure on the concentrations of carbonate species.

5.3: Effect of Salinity

In these simulations, temperature, initial pH and CO_2 injection pressure are constant at 45°C, 7.5 and 160 bar, respectively. Three sets of simulations are performed for brine salinities of 5%, 10% and 15%.

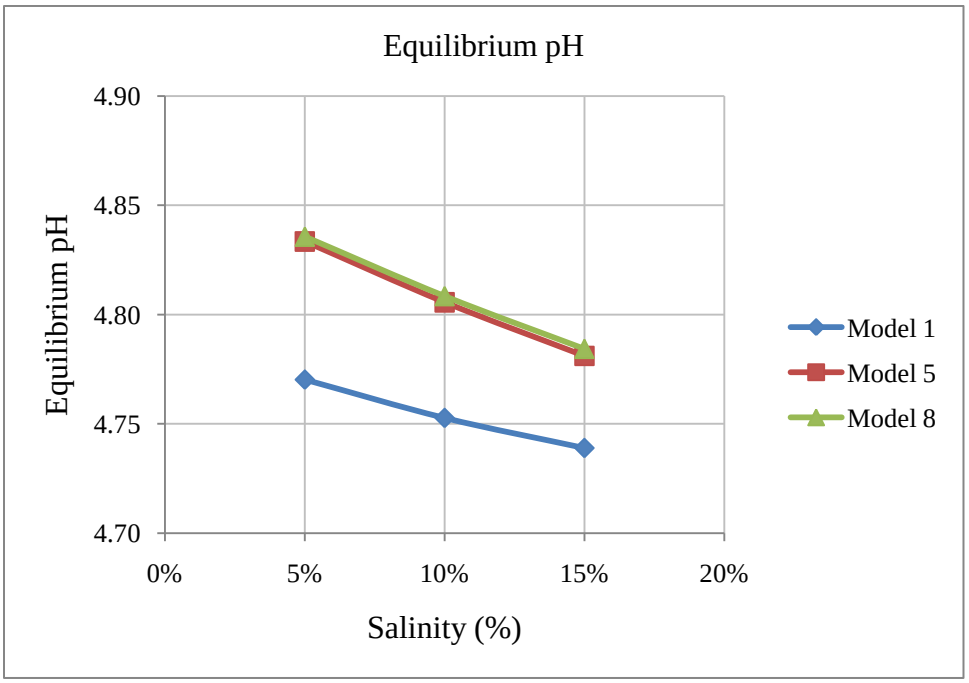

Figure 24: Equilibrium pH as a Function of Salinity

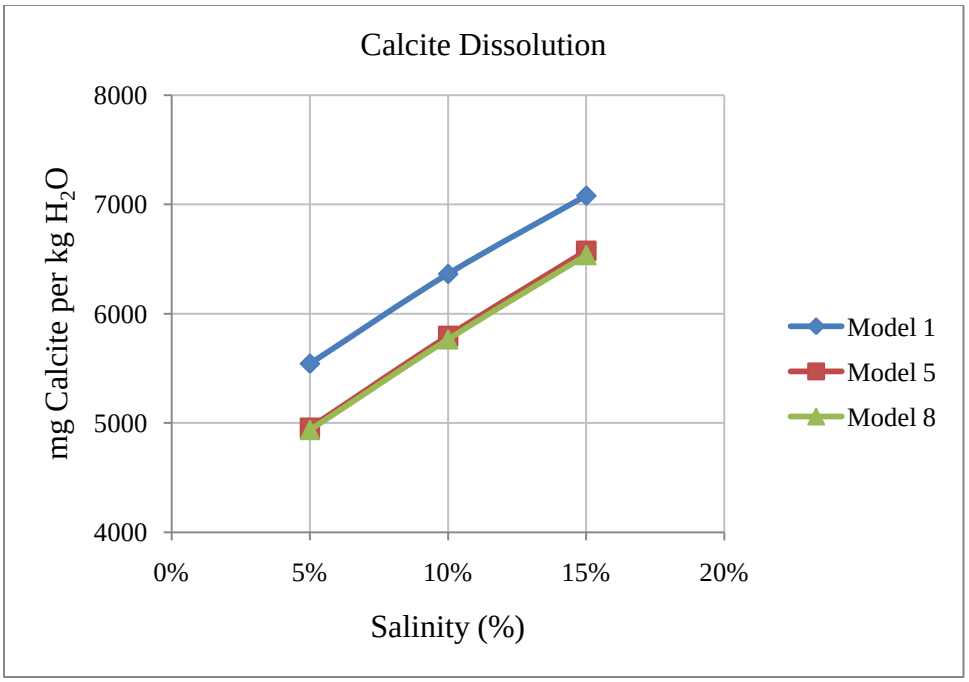

Figure 25: Calcite Dissolution as a Function of Salinity

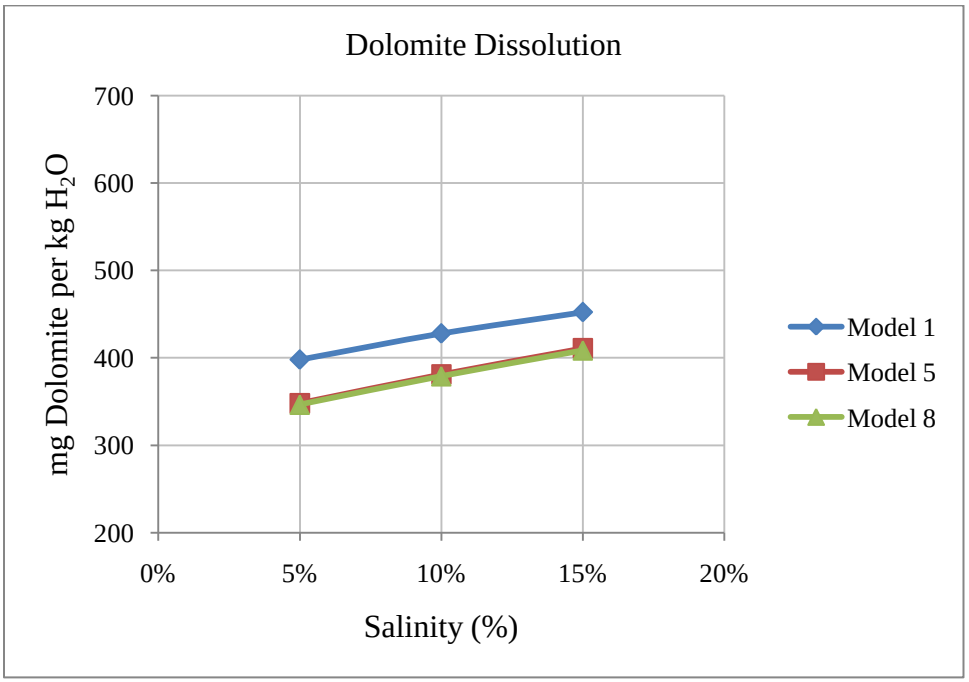

Figure 26: Dolomite Dissolution as a Function of Salinity

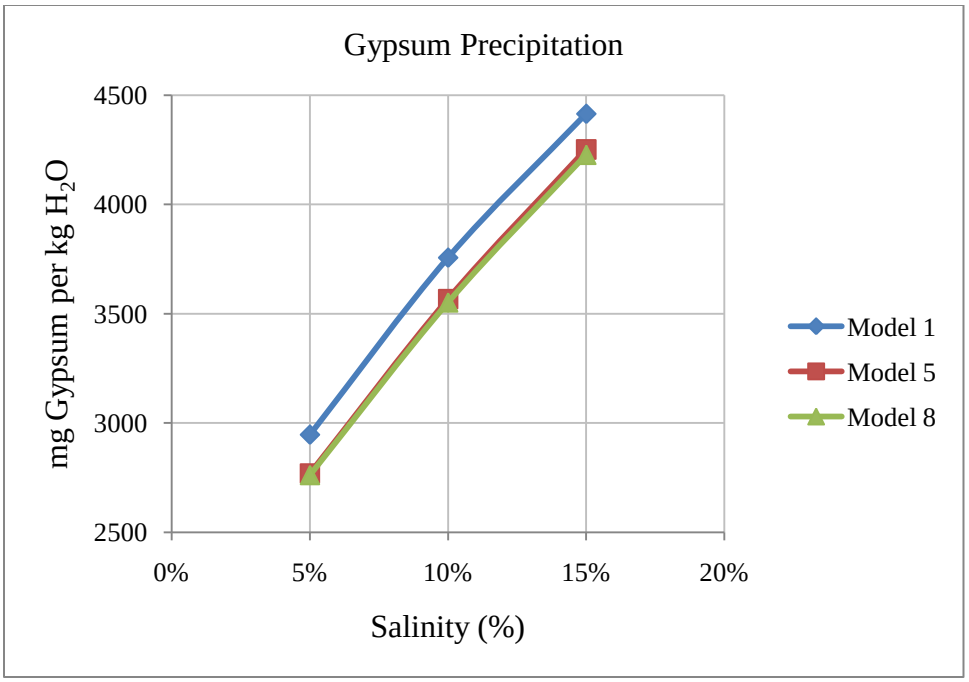

Figure 27: Gypsum Precipitation as a Function of Salinity

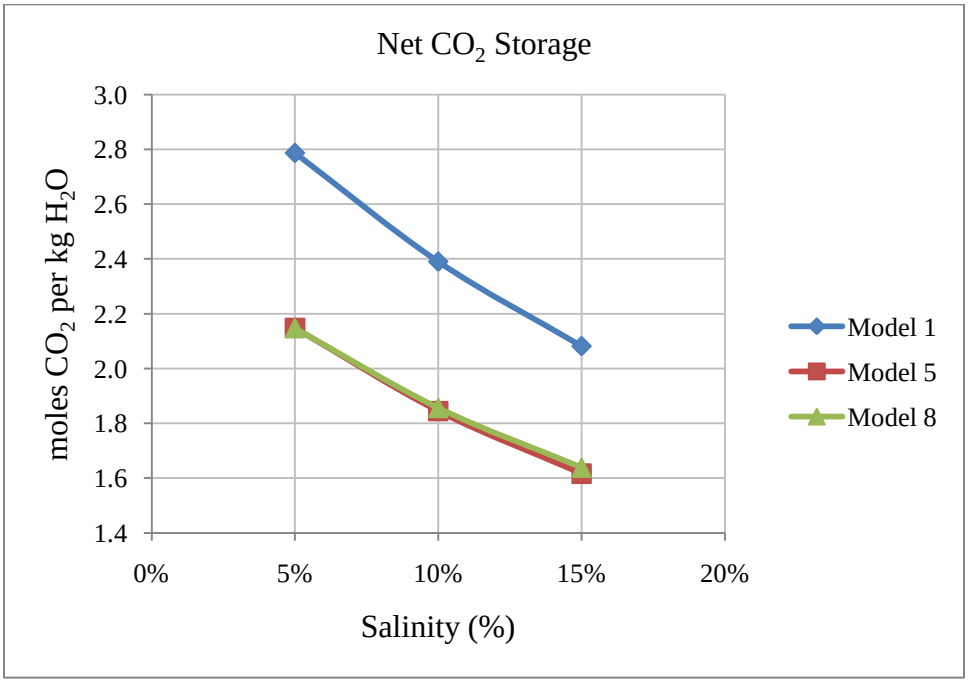

Figure 28: Net CO_2 Storage as a Function of Salinity

The geochemical system appears to be sensitive to salinity, with increasing salinity resulting in increasing quantities of mineral dissolution and precipitation, decreasing equilibrium pH, and decreasing net CO_2 storage. The sensitivity of mineral dissolution and precipitation and equilibrium pH to salinity is due to decreasing estimates for activity coefficients at higher ionic strengths. A lower activity coefficient means that more of a certain ion must be in solution for a given activity required for equilibrium than for a higher activity coefficient; in other words, it takes more of a certain ion to exert the same thermodynamic influence on the solution with a lower activity coefficient than with a higher activity coefficient. These increased ion concentrations thus require proportionally more minerals dissolution. Salinity has the greatest effect on net CO_2 storage out of all the physical and chemical parameters examined. The sensitivity of net CO_2 storage to salinity is due to the decreasing solubility of CO_2 in higher salinity solutions because of the salting out mechanism.

5.4: Effect of Temperature

In these simulations, initial pH, CO_2 injection pressure and salinity are constant at 7.5, 160 bar and 10%, respectively. Three sets of simulations are performed at temperature of 35, 45 and 55°C.

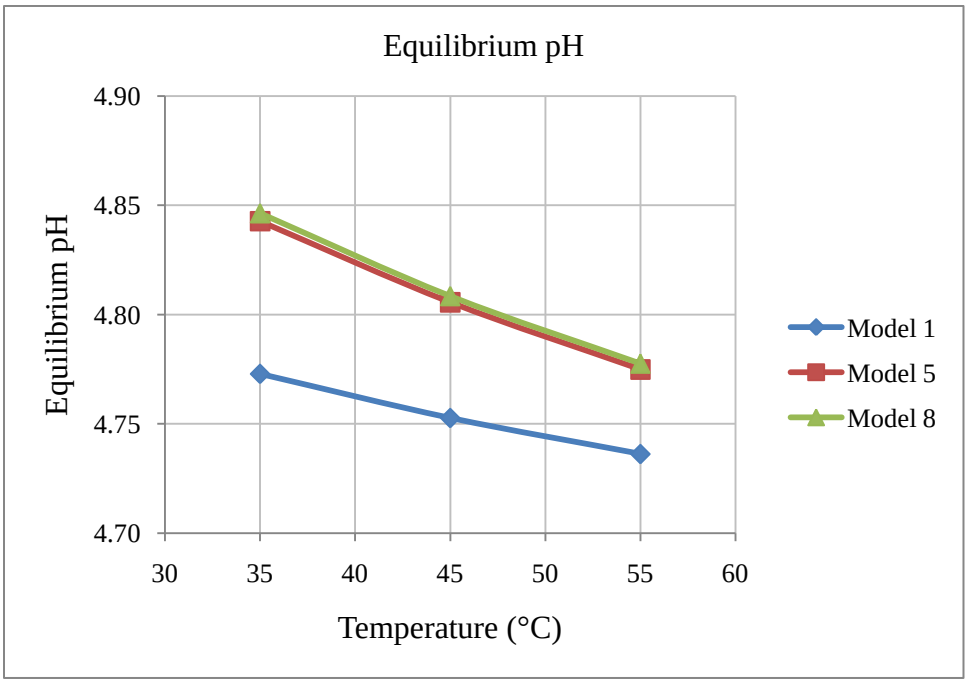

Figure 29: Equilibrium pH as a Function of Temperature

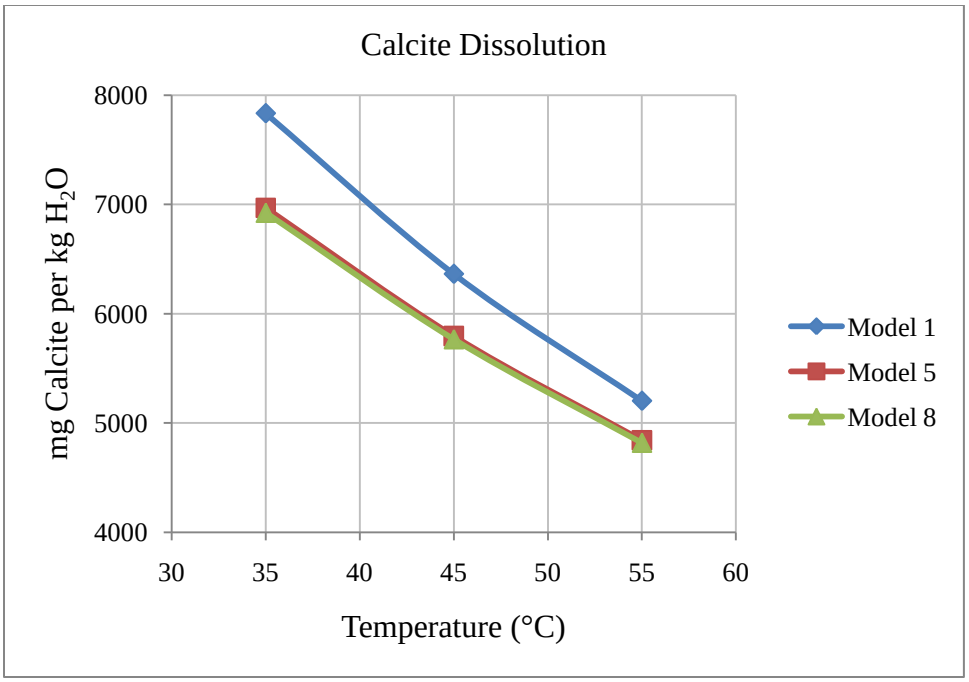

Figure 30: Calcite Dissolution as a Function of Temperature

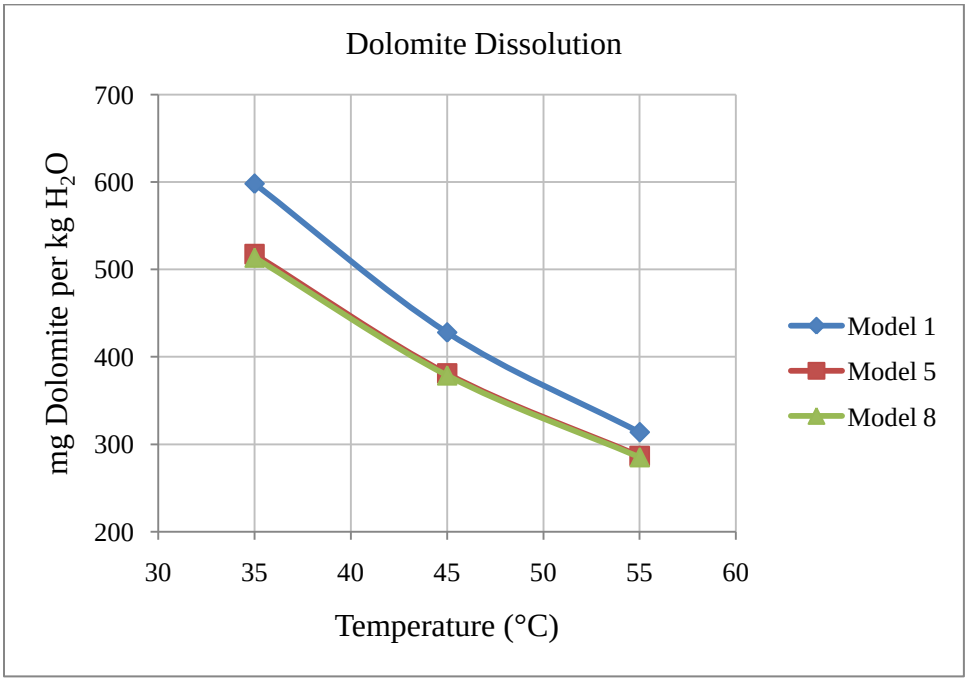

Figure 31: Dolomite Dissolution as a Function of Temperature

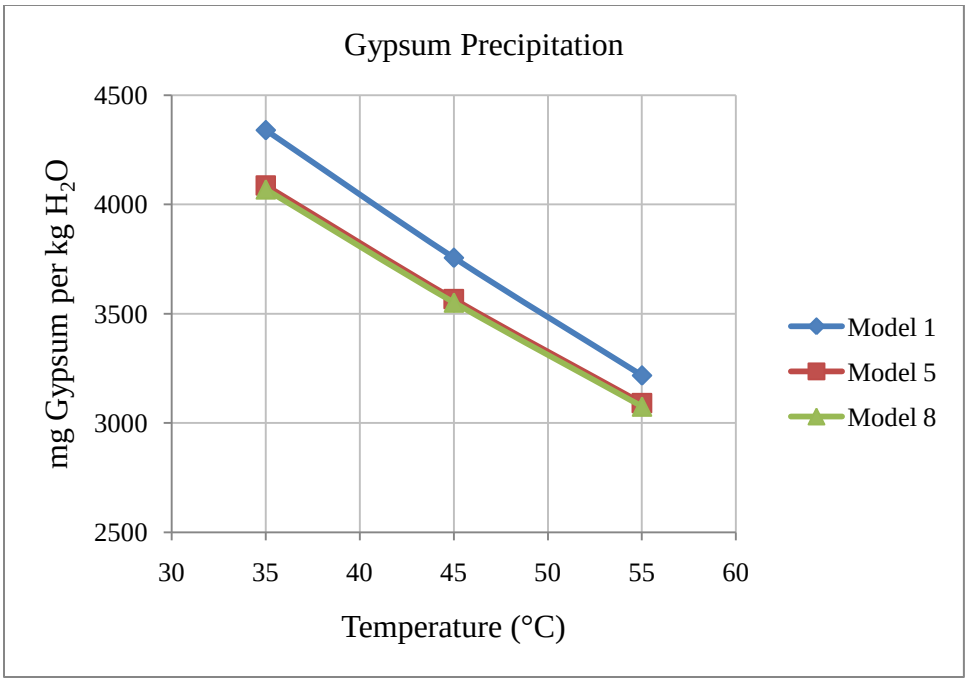

Figure 32: Gypsum Precipitation as a Function of Temperature

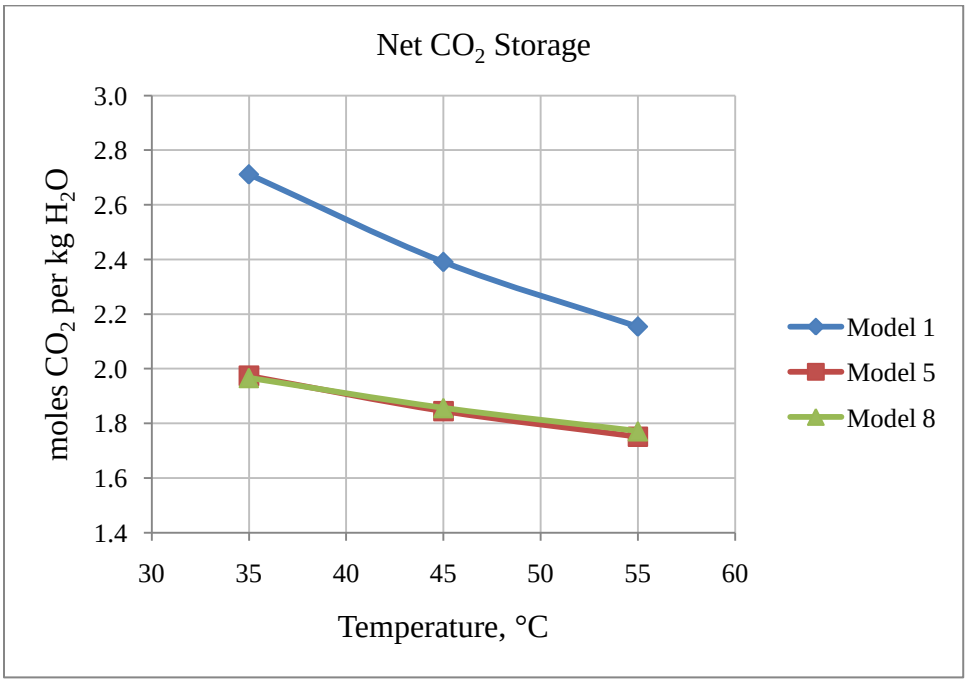

Figure 33: Net CO_2 Storage as a Function of Temperature

The geochemical system appears to be relatively sensitive to temperature, with increasing temperature resulting in decreasing quantities of mineral dissolution and precipitation, decreasing equilibrium pH, and decreasing net CO_2 storage. Sensitivity to temperature is due to decreasing equilibrium constants at higher temperatures for the geochemical reactions considered (see Table 1-Table 4). This effect, known as retrograde solubility, is particularly pronounced with calcium carbonate ($CaCO_{3(s)}$). This means that less free ions must be in solution to achieve equilibrium with the solid mineral phase and the injected CO_2 phase. The decrease in equilibrium pH associated with increased temperatures is also due to the decreased equilibrium constant for the dissociation of water. In other words, at elevated temperatures, the activity of H^+ ions is increased relative to standard conditions.

5.5: Effects on Porosity, ε

The formation porosity, ε, is the ratio of void volume to bulk aquifer volume, and can change as a result of mineral precipitation and dissolution due to CO_2 injection. If significant amounts of minerals dissolve, then porosity will increase. Conversely, if mineral precipitation is the dominant effect, then porosity will decrease. For simplicity, geochemical reactions occurring in the brine that is being displaced by the moving CO_2 interface are not considered. Rather, only the residual pore brine that is not displaced by the moving CO_2 interface – i.e. it is held in place due to capillary forces – is considered to reach equilibrium with the CO_2 phase. The change in porosity can be estimated as follows:

$$\Delta\varepsilon = \varepsilon_{initial} \times S_{RES} \times (1 - S) \times \rho_{BRINE} \times \Delta V_{minerals} \quad \text{Equation 58}$$

where $\varepsilon_{initial}$ is the initial porosity (i.e., before CO_2 injection), S_{RES} is the residual brine saturation of the pore volume, S is the salinity, ρ_{BRINE} is the density of the brine, and $\Delta V_{minerals}$ is the change in mineral volume per kg of H_2O. To estimate $\Delta V_{minerals}$, the following expression is used:

$$\Delta V_{minerals} = \sum \frac{\Delta mineral}{\rho_{mineral}} \quad \text{Equation 59}$$

where $\Delta mineral$ is the net mass of mineral precipitated/dissolved per kg H_2O and $\rho_{mineral}$ is the respective mineral density.

Brine density is estimated and values are tabulated in the following table for various combinations of salinity and temperature (28).

Table 6: Brine Densities at Various Salinities and Temperatures

	Density (kg/m^3)		
Salinity (%)	35 °C	45 °C	55 °C
5	1,031	1,027	1,022
10	1,069	1,065	1,060
15	1,109	1,104	1,099

Mineral densities are estimated using the molecular weights and molar volumes in the TOUGHREACT thermodynamic database (16) for each respective mineral using the following relationship:

$$\rho = \frac{MW}{MV} \qquad \text{Equation 60}$$

where *MW* indicates the molecular weight in g/mole and *MV* indicates the molar volume in cm^3/mole for respective mineral. Calculated densities for calcite, dolomite, and gypsum are listed in the following table:

Table 7: Mineral Densities

Mineral	Density (g/cm^3)
Calcite	2.71
Dolomite	2.86
Gypsum	2.31

The following three combinations of porosity and residual brine saturations are examined:

Table 8: Porosity and Residual Brine Saturation Scenarios

Scenario	$\varepsilon_{INITIAL}$	S_{RES}
1	0.1	0.1
2	0.2	0.3
3	0.3	0.5

Using the three scenarios of porosity and residual brine saturation listed in Table 8, the change in porosity is calculated for the base geochemical scenario described earlier in this chapter with varying initial pH, CO_2 injection pressure, salinity and temperature. Results are given in Table 9.

Table 9: Change in Porosity for Scenarios 1-3 Using Various Combinations of Initial pH, CO_2 Injection Pressure, Salinity, Temperature

Scenario	$\varepsilon_{INITIAL}$	S_{RES}	Init. pH	CO_2 Injection Pressure (bar)	Salinity	Temp. (°C)	Estimated Δε		
							Model 1	Model 5	Model 8
1	0.1	0.1	6.5	160	10%	45	8.3E-06	6.9E-06	6.8E-06
1	0.1	0.1	7.5	160	10%	45	8.3E-06	6.9E-06	6.9E-06
1	0.1	0.1	8.5	160	10%	45	8.3E-06	6.9E-06	6.9E-06
1	0.1	0.1	7.5	120	10%	45	8.0E-06	7.3E-06	7.2E-06
1	0.1	0.1	7.5	200	10%	45	8.4E-06	6.6E-06	6.5E-06
1	0.1	0.1	7.5	160	5%	45	8.8E-06	7.3E-06	7.3E-06
1	0.1	0.1	7.5	160	15%	45	8.0E-06	6.8E-06	6.8E-06
1	0.1	0.1	7.5	160	10%	35	1.2E-05	9.4E-06	9.3E-06
1	0.1	0.1	7.5	160	10%	55	6.0E-06	5.2E-06	5.2E-06
2	0.2	0.3	6.5	160	10%	45	5.0E-05	4.1E-05	4.1E-05
2	0.2	0.3	7.5	160	10%	45	5.0E-05	4.2E-05	4.1E-05
2	0.2	0.3	8.5	160	10%	45	5.0E-05	4.2E-05	4.1E-05
2	0.2	0.3	7.5	120	10%	45	4.8E-05	4.4E-05	4.3E-05
2	0.2	0.3	7.5	200	10%	45	5.0E-05	4.0E-05	3.9E-05
2	0.2	0.3	7.5	160	5%	45	5.3E-05	4.4E-05	4.4E-05
2	0.2	0.3	7.5	160	15%	45	4.8E-05	4.1E-05	4.1E-05
2	0.2	0.3	7.5	160	10%	35	7.0E-05	5.7E-05	5.6E-05
2	0.2	0.3	7.5	160	10%	55	3.6E-05	3.1E-05	3.1E-05
3	0.3	0.5	6.5	160	10%	45	1.2E-04	1.0E-04	1.0E-04
3	0.3	0.5	7.5	160	10%	45	1.2E-04	1.0E-04	1.0E-04
3	0.3	0.5	8.5	160	10%	45	1.2E-04	1.0E-04	1.0E-04
3	0.3	0.5	7.5	120	10%	45	1.2E-04	1.1E-04	1.1E-04
3	0.3	0.5	7.5	200	10%	45	1.3E-04	9.9E-05	9.8E-05
3	0.3	0.5	7.5	160	5%	45	1.3E-04	1.1E-04	1.1E-04
3	0.3	0.5	7.5	160	15%	45	1.2E-04	1.0E-04	1.0E-04
3	0.3	0.5	7.5	160	10%	35	1.8E-04	1.4E-04	1.4E-04
3	0.3	0.5	7.5	160	10%	55	9.1E-05	7.8E-05	7.8E-05

Estimates for the change in porosity are positive (i.e., porosity *increases*) for all models and are virtually identical for models 5 and 8 and model 1 agreeing within 20%.

The change in porosity is strongly related to the initial porosity and residual brine saturation, with estimates spanning three orders of magnitude for initial porosity ranging from 0.1 to 0.3 and residual brine saturation ranging from 0.1 to 0.5. Specifically, higher initial porosity and residual brine saturation results in larger estimated changes in porosity for the geochemical system considered. This is because higher initial porosity and residual brine saturation implies that there is more brine available per unit aquifer volume for equilibration with surrounding minerals and the injected CO_2, resulting in larger net mineral dissolution and precipitation quantities per unit aquifer volume. However, the overall change in porosity is very small for all scenarios considered, with a maximum change that is three orders of magnitude less than the initial porosity. This agrees well with observations by others (5; 7).

5.6: Choice of Thermodynamic Sub-model for CO_2 Parameter Estimation

In every simulation, model 1 gave the largest net mineral reactions and change in pH. This is most likely due to the greater fugacity coefficient predicted using the method of Spycher and Reed (26) and the higher aqueous CO_2 concentration predicted using the equilibrium constant method. Models 5 and 8 use more recently developed correlations that account for the effects of dissolved salts to estimate the equilibrium dissolved CO_2 concentration, and the lower estimated aqueous CO_2 concentrations result in slightly lower net mineral reactions and changes in pH as compared to model 1. However, estimates of mineral precipitation and dissolution are closely grouped within the same order of magnitude for all three models, indicating that the choice of thermodynamic sub-models does not have a significant impact on the estimated quantities.

6: Summary and Conclusion

Different thermodynamic sub-models are used to construct overall geochemical models to describe pre- and post- CO_2 injection conditions in a deep, saline aquifer that is comprised of calcite, dolomite, and gypsum. It is found that the overall geochemical models are relatively insensitive to appropriate choices for thermodynamic sub-models for estimating such parameters as $CO_{2(aq)}$ activity coefficient, $CO_{2(g,sc)}$ fugacity coefficient, and the solubility of $CO_{2(aq)}$. These geochemical models are used to determine concentrations of ionic species and aqueous complexes and quantify the amount of minerals that are dissolving into or precipitating out of solution so that the change in porosity due to CO_2 injection can be estimated. All of the models predict that calcite and dolomite will dissolve and gypsum will precipitate. The models all predict that CO_2 storage by solubility trapping is likely, but carbonate mineral dissolution under acidic conditions prevents mineral trapping.

It is determined that mineral dissolution and precipitation, along with requisite changes in porosity, are relatively sensitive to the temperature and salinity of the native brine in the aquifer and relatively insensitive to the CO_2 injection pressure and initial pH of the brine. However, over the range of conditions examined, the estimated net change in porosity is low, with a maximum increase of magnitude 10^{-4} and a minimum increase of magnitude 10^{-6}. It appears that CO_2 injection and storage in deep, saline aquifers comprised of calcite, dolomite, and gypsum for the physical and chemical conditions considered will have little effect on the formation porosity.

Works Cited

1. CO_2 storage in geological media: Role, means, status and barriers to deployment. Bachu, Stefan. 2008. Progress in Energy and Combustion Science, Vol. 34, pp. 254-273.

2. Carbon Dioxide Capture and Storage. Intergovernmental Panel on Climate Change. Cambridge University Press, 2005.

3. Mineral sequestration of carbon dioxide in a sandstone-shale system. Xu, Tianfu, Apps, John A and Pruess, Karsten. 2004. Chemical Geology, Vol. 217, pp. 295-318.

4. Numerical modeling of fluid-rock chemical interactions at the supercritical CO_2-liquid interface during CO_2 injection into a carbonate reservoir, the Dogger aquifer (Paris Basin, France). Andre, L, Audigane, P and Menjoz, A. 2007. Energy Conversion & Management, Vol. 48, pp. 1782-1797.

5. Reactive Transport Modeling of CO_2 Sequestration in Deep Saline Aquifers. Lagneau, V., Pipart, A. and Catalette, H. 2005, Oil & Gas Science and Technology, Vol. 60, pp. 231-247.

6. CO_2 injection into saline carbonate aquifer formations I: laboratory investigation. Izgec, Omer, Demiral, Birol, Bertin, Henri and Akin, Serhat. 2007. Transport in Porous Media, Vol. 72, pp. 1-24.

7. Evaluation of Subsurface Sequestration of Carbon Dioxide (CO_2) at the Polk Power Station: Physical and Chemical Modeling. Cunningham, Jeffrey, Stewart, Mark, Okwen, Roland and Thomas, Mark. 2010. Report to TECO Energy.

8. Evaluation of Subsurface Sequestration of Carbon Dioxide (CO_2) at the Polk Power Station: Physical and Chemical Modeling Phase III: Detailed Physical Modeling. Cunningham, Jeffrey, Stewart, Mark and Okwen, Roland. 2008. Report to TECO Energy.

9. Evaluation of Subsurface Sequestration of Carbon Dioxide (CO_2) at the Polk Power Station: Physical and Chemical Modeling Phase II: Preliminary Physical Modeling. Cunningham, Jeffrey, Stewart, Mark and Okwen, Roland. 2007. Report to TECO Energy.

10. Demonstrating storage of CO_2 in geological reservoirs: The Sleipner and SACS projects. Torp, Tore A and Gale, John. 2004. Energy, Vol. 29, pp. 1361-1369.

11. Evaluation of the impact of CO_2, co-contaminant gas, aqueous fluid and reservoir rock interactions on the geologic sequestration of CO_2. Knauss, Kevin G, Johnson, James W and Steefel, Carl I. 2004. Chemical Geology, Vol. 217, pp. 339-350.

12. Numerical modeling of injection and mineral trapping of CO_2 with H_2S and SO_2 in a sandstone formation. Xu, Tianfu, Apps, John A, Pruess, Karsten and Yamamoto, Hajime. 2007. Chemical Geology, Vol. 242, pp. 319-346.

13. Pore Scale Modeling of Reactive Transport Involved in Geologic CO_2 Sequestration. Kang, Qinjun, Lichtner, Peter C, Viswanathan, Hari S and Abdel-Fattah, Amr I. 2010. Transport in Porous Media, Vol. 82.

14. CO_2 Injection into Saline Carbonate Aquifer Formations II: Comparison of Numerical Simulations to Experiments. Izgec, Omer, Demiral, Birol, Bertin, Henri and Serhat, Akin. 2007. Transport in Porous Media, Vol. 73, pp. 57-74.

15. Sequestration of CO_2 in geological media in response to climate change: capacity of deep saline aquifers to sequester CO_2 in solution. Bachu, S. and Adams, J. J. 2003. Energy Conversion and Management, Vol. 44, pp. 3151-3175

16. TOUGHREACT User's Guide: A simulation Program for Non-isothermal Multiphase Reactive Ceochemical Transport in Variably Saturated Geologic Media. Xu, Tianfu, Sonnenthal, Eric, Spycher, Nicolas and Pruess, Karsten. 2004. LBNL-55460

17. Theoretical Prediction of the Thermodynamic Behavior of Aqueous Electrolytes at High Pressures and Temperatures: IV. Calculation of Activity Coefficients, Osmotic Coefficients, and Apparent Molal and Standard and Relative Partial Molal Properties to 600°C. Helgeson, Harold C, Kirkham, David H and Flowers, George C. 1981. American Journal of Science, Vol. 28, pp. 1249-1516.

18. Theoretical Prediction of the Thermodynamic Behavior of Aqueous Electrolytes at High Pressures and Temperatures: II. Debye-Huckel Parameters for Activity Ceofficients and Relative Partial Molal Properties. Helgeson, Harold C and Kirkham, David H. 1974. American Journal of Science, Vol. 274, pp. 1199-1261.

19. Calculation of multicomponent chemical equilibria and reaction processes in systems involving minerals, gases and an aqueous phase. Reed, Mark H. 1982. Geochemica et Cosmochimica Acta, Vol. 46, pp. 513-528.

20. An improved model for the calculation of CO_2 solubility in aqueous solutions containing Na^+, K^+, Ca^{2+}, Mg^{2+}, Cl^-, and SO_4^{2-}. Duan, Zhenhao, Sun, Rui, Zhu, Chen and Chou, I-Ming. 2006. Marine Chemistry, Vol. 98, pp. 131-139.

21. CO_2-H_2O mixtures in the geological sequestration of CO_2. II. Partitioning in chloride brines at 12-100°C and up to 600 bar. Spycher, Nicolas and Pruess, Karsten. 2005. Geochimica et Cosmochimica Acta, Vol. 69, pp. 3309-3320.

22. Boiling and mixing of hydrothermal fluids: Chemical effects on mineral precipitation. Drummond, J. M. 1981. Ph.D. Thesis, The Pennsylvania State University, University Park, Pennsylvania.

23. Solubility of Carbon-Dioxide in Aqueous Solutions of Sodium-Chloride - Experimental Results and Correlation. Rumpf, B, Nicolaisen, H, Ocal, C and Maurer, G. 1994. Journal of Solution Chemistry, Vol. 23, pp. 431-448.

24. An equation of state for the CH_4-CO_2-H_2O system: I. Pure systems from 0 to 1000°C and 0 to 8000 bar. Duan, Zhenhao, Moller, Nancy and Weare, John H. 1992. Geochimica et Cosmochimica Acta, Vol. 56, pp. 2605-2617.

25. An improved model calculating CO_2 solubility in pure water and aqueous NaCl solutions from 273 to 533 K and from 0 to 2000 bar. Duan, Zhenhao and Sun, Rui. 2003. Chemical Geology, Vol. 193, pp. 257-271.

26. Fugacity coefficients of H_2, CO_2, CH_4, H_2O and of H_2O-CO_2-CH_4 mixtures: A virial equation treatment for moderate pressures and temperatures applicable to calculations of hydrothermal boiling. Spycher, Nicolas F and Reed, Mark H. 1988. Geochimica et Cosmochimica Acta, Vol. 52, pp. 739-749.

27. CO_2-H_2O mixtures in the geological sequestration of CO_2. I. Assessment and calculation of mutual solubilities from 12 to 100°C and up to 600 bar. Spycher, Nicolas, Pruess, Karsten and Ennis-King, Jonathen. 2003. Geochimica et Cosmochimica Acta, Vol. 67, pp. 3015-3031.

28. Algorithms for computation of fundamental properties of seawater. Fofonoff, N. P. and Millard Jr., R. C. UNESCO, 1983.